Chapter 10
Scour

10.1 General

Scour is a natural phenomenon of lowering the riverbed level due to removal of sediment by the erosive action of flowing stream. The magnitude of reduction in the riverbed level below an assumed natural level (or initial level) is termed *scour depth*. Scour is broadly classified as *general scour*, *contraction scour*, and *local scour*.

General scour in the river occurs as a result of the change in characteristics of the river. Based on the duration of scour development, general scour can be categorized as short-term scour and long-term scour. *Short-term scour* occurs during a single flood or several floods of shorter durations to appear in quick succession, while *long-term scour* takes a considerably long time, usually of the order of a number of years, and results in a progressive bed degradation and bank erosion. Short-term scour may also occur due to flow convergence, a shift in the meandering stream thalweg or braids within the stream and bedform migration. On the other hand, the long-term scour may be caused by the natural changes in the catchments, for example, channel straightening, volcanic activities, climate change, or by the human activities, for example, channel alterations, streambed mining, dam/reservoir construction, and land-use changes.

Contraction scour is the scour of streambed arising from accelerated flow through contraction of waterways, where flows over flood plains are converged by bridge causeways and channeled through the bridge waterways.

In contrast, *local scour* (also termed *localized scour*) is developed near the structures due to modification of the flow field as a result of obstruction to the flow by the structures. Scour within the contracted portion of rivers, scour downstream of structures, scour at bed sills, scour below horizontal pipelines, scour at bridge piers and abutments, and scour at other river training works are the examples of local scour.

Local scour is classified as clear-water scour and live-bed scour. *Clear-water scour* occurs when the sediment is removed from the scour hole but not supplied by the approaching flow. The equilibrium of scour is reached when the flow induced

force can no longer dislodge the sediment particles from the scour hole. On the other hand, *live-bed scour* occurs when the scour hole is continuously fed with the sediment by the approaching flow. The equilibrium of scour is attained over a period of time, when the rate of removal of sediment out of the scour hole equals the rate of supply of sediment into the scour hole. Usually, the magnitude of scour depth in live bed is to some extent less than that in clear-water, if the flow condition is such that the approaching flow velocity U equals or is slightly less the threshold flow velocity U_{cr} for the bed sediment motion.

This chapter summarizes the contraction scour and local scour at different structures including various aspects, such as mechanism of scour and design formulas for the prediction of scour depth. It is however pertinent to mention that despite large number of investigations, hydraulics of local scour is as yet not well established, because most of the studies came from the laboratory and only a few from the fields. As such, the scour prediction formulas can only provide a general guideline for the designers or engineers.

10.2 Scour Within Channel Contractions

A reduction in width of a watercourse by constructing parallel sidewalls is termed *channel contraction*. Contractions of river width to construct bridges, barrages, weirs, and cross-drainage works are common examples of channel contractions. The flow velocity in the contracted zone of the channel increases due to the reduction in flow area, and hence, the bed shear stress induced by the flow increases considerably. Consequently, the sediment bed within the channel contraction is scoured. Such localized scour in the contracted zone of the channel is called *contraction scour*.

Depending on the ratio of the length of the contraction L to the approaching channel width B_1, channel contractions are designated as long or short. According to Komura (1966) and Dey and Raikar (2005), a contraction becomes long when $L/B_1 > 1$, whereas Webby (1984) considered it as $L/B_1 > 2$. Figures 10.1 and 10.2 show schematic of scour in a channel contraction and a photograph of the scoured bed, respectively. Smith (1967) proposed the angles of upstream and downstream transitions as 12.5° for a smooth transition to the contracted zone.

Local scour in a channel contraction is usually studied considering a configuration of long rectangular contraction, as shown schematically in Fig. 10.1. Because of the simple geometrical configuration of the problem, various analytical investigations to predict the equilibrium scour depth in long contractions were attempted. Straub (1934) was the pioneer to present a simplified one-dimensional theory of the equilibrium scour in long contractions. His work was later extended and modified by Laursen (1963), Komura (1966), Gill (1981), Lim (1993), and Lim and Cheng (1998). Further, Dey and Raikar (2005, 2006) studied the scour in long contractions in gravel-beds and proposed analytical models for the estimation of scour depth under both clear-water and live-bed scour conditions.
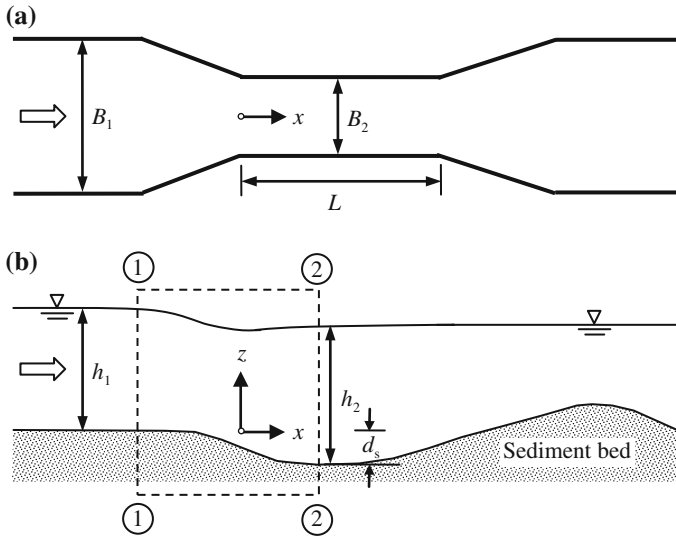
Fig. 10.1 Schematic of a rectangular channel contraction at equilibrium scour condition: **a** *plan view* and **b** *elevation view*

Fig. 10.2 Photograph showing an equilibrium scoured bed within a channel contraction

10.2.1 Laursen's Model

Laursen (1963) considered a channel contraction as shown in Fig. 10.1. The discharge in the channel is obtained from the continuity equation as

$$Q = U_1 h_1 B_1 = U_2 h_2 B_2 \tag{10.1}$$

where U_1 is the approaching flow velocity, h_1 is the approaching flow depth, U_2 is the flow velocity in contracted zone, h_2 is the flow depth in contracted zone, and B_2 is the contracted width of the channel.

Using the energy equation between sections 1 and 2, the scour depth d_s is obtained as

$$h_1 + \frac{U_1^2}{2g} = h_2 + \frac{U_2^2}{2g} - d_s + h_f \quad \wedge \quad h_f = K_L \left(\frac{U_2^2}{2g} - \frac{U_1^2}{2g} \right) \tag{10.2a}$$

$$\Rightarrow \frac{d_s}{h_1} = \frac{h_2}{h_1} - 1 + \left(\frac{1 + K_L}{2} \right) Fr_1^2 \left[\left(\frac{B_1}{B_2} \right)^2 \left(\frac{h_1}{h_2} \right)^2 - 1 \right] \tag{10.2b}$$

where h_f is the head loss due to flow in transition, Fr_1 is the approaching flow Froude number [$= U_1/(gh_1)^{0.5}$], and K_L is the head loss coefficient.

When the scour in the contracted zone reaches an equilibrium, the bed shear stress becomes equal to its threshold value, that is, $\tau_{0c} = 0.628 d_{50}$ (in Pa), where d_{50} is the median sediment size (in mm). The bed shear stress τ_{01} in the uncontracted zone (section 1) can be estimated using the Manning equation and the Strickler's relationship for Manning roughness coefficient n as

$$\tau_{01} = \frac{U_1^2 d_{50}^{0.33}}{30 h_1^{0.33}} \tag{10.3}$$

Taking the ratio of bed shear stress in the uncontracted zone to that in the contracted zone yields

$$\frac{\tau_{01}}{\tau_{0c}} = \frac{U_1^2}{120 d_{50}^{2/3} h_1^{1/3}} \tag{10.4}$$

Similar expression can also be written for the bed shear stress in the contracted zone. Hence, the flow depth ratio h_2/h_1 can be obtained from

$$\frac{\tau_{01}}{\tau_{02}} = \left(\frac{U_1}{U_2} \right)^2 \left(\frac{h_2}{h_1} \right)^{1/3} = \frac{\tau_{01}}{\tau_{0c}} \tag{10.5}$$

where τ_{02} is the bed shear stress in the contracted zone (section 2).

Using Eqs. (10.1) and (10.5), one can write

$$\frac{h_2}{h_1} = \left(\frac{\tau_{01}}{\tau_{0c}} \right)^{3/7} \left(\frac{B_1}{B_2} \right)^{6/7} \tag{10.6}$$

Substituting Eq. (10.6) into Eq. (10.2b) results

$$\frac{d_s}{h_1} = \left(\frac{\tau_{01}}{\tau_{0c}}\right)^{3/7}\left(\frac{B_1}{B_2}\right)^{6/7} - 1 + 1.87(1 + K_L)\left(\frac{d_{50}}{h_1}\right)^{2/3}\left[\frac{(B_1/B_2)^{2/7}}{(\tau_{01}/\tau_{0c})^{6/7}} - 1\right]\left(\frac{\tau_{01}}{\tau_{0c}}\right)$$

(10.7)

Neglecting the difference in the velocity heads and the loss through the transition, Eq. (10.7) reduces to

$$\frac{d_s}{h_1} = \left(\frac{\tau_{01}}{\tau_{0c}}\right)^{3/7}\left(\frac{B_1}{B_2}\right)^{6/7} - 1$$

(10.8)

10.2.2 Dey and Raikar's Model

Dey and Raikar (2005, 2006) developed analytical models for clear-water and live-bed scour cases.

10.2.2.1 Clear-Water Scour Model

Dey and Raikar (2005) analytically computed the equilibrium clear-water scour depth in two ways: Considering sidewall correction and without considering sidewall correction.

Determination of scour depth considering sidewall correction: In clear-water scour, the equilibrium scour depth d_s reaches in a long contraction, when the flow velocity U_2 in the contracted zone becomes equal to threshold velocity U_{cr} for the sediment motion. The flow velocity $U_2|_{U_2=U_{cr}}$ in the contracted zone can be obtained from the well-known equation of bed shear stress as a function of dynamic pressure (Eq. 3.54). It is

$$\tau_{0c}(= \rho u_{*c}^2) = \frac{\lambda_D}{8}\rho U_2|_{U_2=U_{cr}}^2 \Rightarrow U_2|_{U_2=U_{cr}} = u_{*c}\left(\frac{8}{\lambda_D}\right)^{0.5}$$

(10.9)

where ρ is the mass density of water, u_{*c} is the threshold shear velocity for sediment, and λ_D is the Darcy–Weisbach friction factor, which can be determined from Colebrook–White equation (Eq. 3.55).

In the contracted zone, the bed is rough consisting of sediment particles and the sidewalls are smooth. Hence, the friction factor $\lambda_D|_w$ associated with the wall is considerably different from the friction factor $\lambda_D|_b$ associated with the bed. Therefore, Vanoni's (1975) method of sidewall correction can be applied for the contracted zone of the channel, as given in Sect. 3.9, where the solution for $\lambda_D|_b$ was obtained from the solution of Eqs. (3.63) and (3.64), which are here expressed as

$$\lambda_{\mathrm{D}}|_{\mathrm{b}} = 0.316 Re|_{\mathrm{b}} \left(\frac{4U_2|_{U_2=U_{\mathrm{cr}}} A}{\upsilon P|_{\mathrm{w}}} - \frac{Re|_{\mathrm{b}} P|_{\mathrm{b}}}{P|_{\mathrm{w}}} \right)^{-1.25} \tag{10.10a}$$

$$\frac{1}{\lambda_{\mathrm{D}}|_{\mathrm{b}}^{0.5}} = -0.86 \ln \left(\frac{k_{\mathrm{s}} U_2|_{U_2=U_{\mathrm{cr}}}}{3.7 \upsilon Re|_{\mathrm{b}}} + \frac{2.51}{Re|_{\mathrm{b}} \lambda_{\mathrm{D}}|_{\mathrm{b}}^{0.5}} \right) \tag{10.10b}$$

where k_{s} is equivalent roughness height ($=2d_{50}$), $Re|_{\mathrm{b}}$ is the flow Reynolds number associated with the bed, that is, $4U_2|_{U_2=U_{\mathrm{cr}}} A|_{\mathrm{b}}/(\upsilon P|_{\mathrm{b}})$, $A|_{\mathrm{b}}$ is the flow area associated with the bed, $P|_{\mathrm{b}}$ is the wetted perimeter associated with the bed ($=B_2$), A is the total flow area of contracted zone ($=h_2 B_2$), $P|_{\mathrm{w}}$ is the wetted perimeter associated with the wall ($=2h_2$), and υ is the kinematic viscosity of water.

In clear-water scour, at equilibrium scour condition, Eq. (10.1) becomes

$$U_1 h_1 B_1 = U_2|_{U_2=U_{\mathrm{cr}}} h_2 B_2 \tag{10.11}$$

For the given U_1, h_1, B_1, B_2, and d_{50}, the unknowns $U_2|_{U_2=U_{\mathrm{cr}}}$, h_2, $Re|_{\mathrm{b}}$, and $\lambda_{\mathrm{D}}|_{\mathrm{b}}$ can be determined numerically solving Eqs. (10.9), (10.10a, b) and (10.11). Then, neglecting the head loss in transition, energy equation [see the energy equation, Eq. (10.2a)] is used to determine equilibrium scour depth d_{s} as

$$d_{\mathrm{s}} = h_2 + \frac{U_2|_{U_2=U_{\mathrm{cr}}}^2}{2g} - h_1 - \frac{U_1^2}{2g} \tag{10.12}$$

Determination of scour depth without considering sidewall correction: In this simplified approach, the depth-averaged flow velocity $U_2|_{U_2=U_{\mathrm{cr}}}$ in the contracted zone for equilibrium scour is determined assuming the logarithmic equation of the depth-averaged velocity as

$$\frac{U_2|_{U_2=U_{\mathrm{cr}}}}{u_{*\mathrm{c}}} = 5.75 \log \frac{h_2}{2d_{50}} + 6 \tag{10.13}$$

For the given U_1, h_1, B_1, B_2, and d_{50}, the unknowns $U_2|_{U_2=U_{\mathrm{cr}}}$ and h_2 can be obtained numerically solving Eqs. (10.11) and (10.13). Then, equilibrium scour depth d_{s} can be determined from Eq. (10.12).

10.2.2.2 Live-Bed Scour Model

Dey and Raikar (2006) proposed a live-bed scour model for the estimation of scour depth within channel contractions. In live-bed scour, the equilibrium scour depth is reached, when the sediment supplied by the approaching flow into the contracted zone is balanced by the sediment transported out of the contracted zone. Thus, at the equilibrium, the sediment continuity equation between sections 1 and 2 of Fig. 10.1 is

$$q_b|_{u_*=u_{*1}} B_1 = q_b|_{u_*=u_{*2}} B_2 \qquad (10.14)$$

where q_b is the bed-load transport rate of sediment. The bed-load transport rate q_b can be estimated by the formula of Fredsøe and Deigaard (1992) as

$$q_b = 1.55\,\pi\,d_{50}\,u_*\left(1 - 0.7\frac{u_{*c}}{u_*}\right)p \quad \wedge \quad p = \left[1 + \left(\frac{0.085\,\pi\Delta g d_{50}}{u_*^2 - u_{*c}^2}\right)^4\right]^{-0.25} \qquad (10.15)$$

Assuming the logarithmic equation of average velocity for approaching flow, the shear velocity u_{*1} at section 1 is obtained as

$$u_{*1} = U_1\left(5.75\log\frac{h_1}{2d_{50}} + 6\right)^{-1} \qquad (10.16)$$

In the contracted zone, incorporating the logarithmic equation of average velocity in Eq. (10.1) yields

$$\frac{B_1}{B_2}\cdot\frac{h_1}{h_2} = \frac{u_{*2}}{U_1}\left(5.75\log\frac{h_2}{2d_{50}} + 6\right) \qquad (10.17)$$

where u_{*2} is the shear velocity in the contracted zone.

For the given U_1, h_1, B_1, B_2, and d_{50}, the unknowns U_2 and h_2 can be determined numerically solving Eqs. (10.14), (10.15) and (10.17). Then, the energy equation [see the energy equation, Eq. (10.2a)] is used to determine equilibrium scour depth d_s as

$$d_s = h_2 - h_1 + \frac{U_2^2}{2g} - \frac{U_1^2}{2g} \qquad (10.18)$$

10.2.3 Maximum Scour Depth Prediction

The parameters that influence the scour within channel contractions are as follows (Dey and Raikar 2005):

1. *Parameters relating to the channel contraction*: Channel opening ratio and channel shape.
2. *Parameters relating to the bed sediment*: Median particle size, particle size distribution, angle of repose, and cohesiveness.
3. *Parameters relating to the approaching flow condition*: Approaching flow velocity, approaching flow depth, shear velocity, and roughness.

4. *Parameters relating to the fluid*: Mass density, viscosity, gravitational acceleration, and temperature. Note that the temperature may not be important in scour problems, unless free surface is frozen.

The functional relationship showing the influence of above parameters on the equilibrium scour depth d_s in a long rectangular contraction can be given as

$$d_s = d_s(U_1, h_1, \rho, \rho_s, g, \upsilon, d_{50}, B_1, B_2, \sigma_g) \tag{10.19}$$

where ρ_s is the mass density of sediment, g is the gravitational acceleration, and σ_g is the geometric standard deviation of the particle size distribution.

Dey and Raikar (2005) argued that the scour in a long contraction starts when the excess approaching flow velocity $U_{1e}(= U_1 - U_1|_{U_2=U_{cr}}^{d_s=0})$ is greater than zero. For no-scour condition, U_{1e} is less than or equal to zero. Here, $U_1|_{U_2=U_{cr}}^{d_s=0}$ refers to the approaching flow velocity U_1 that initiates scour in a contraction. Therefore, $U_1|_{U_2=U_{cr}}^{d_s=0}$ corresponds to U_1 for which U_2 becomes U_{cr} for the undisturbed bed condition ($d_s = 0$) in the contracted zone. The $U_1|_{U_2=U_{cr}}^{d_s=0}$ can be determined as follows:

Considering negligible head loss ($h_f = 0$) and applying the energy equation between sections 1 and 2 for the bed sediments within contracted zone under threshold condition, that is $U_2 = U_{cr}$, before initiation of scour ($d_s = 0$), the following equation is obtained (Fig. 10.1) (Dey and Raikar 2005):

$$h_1 + \frac{1}{2g}\left(U_1|_{U_2=U_{cr}}^{d_s=0}\right)^2 = h_2 + \frac{1}{2g}\left(U_2|_{U_2=U_{cr}}^{d_s=0}\right)^2 \tag{10.20}$$

The continuity equation between sections 1 and 2 is

$$U_1|_{U_2=U_{cr}}^{d_s=0}h_1B_1 = U_2|_{U_2=U_{cr}}^{d_s=0}h_2B_2 \tag{10.21}$$

The threshold flow velocity at section 2 can be determined using the logarithmic equation of average velocity as

$$\frac{U_2|_{U_2=U_{cr}}^{d_s=0}}{u_{*c}} = 5.75\log\frac{h_2}{2d_{50}} + 6 \tag{10.22}$$

Therefore, for the given h_1, B_1, B_2, d_{50}, and u_{*c} (determined from the Shields diagram), the approaching flow velocity $U_1|_{U_2=U_{cr}}^{d_s=0}$ required to initiate the sediment motion within the contracted zone can be estimated solving Eqs. (10.20)–(10.22) numerically.

In the context of scour, it is appropriate that U_1, in Eq. (10.19), is to be replaced by U_{1e}. In sediment–water interaction, the parameters g, ρ, and ρ_s are combined into a parameter Δg, where $\Delta = s - 1$ and s is the relative density of sediment ($= \rho_s/\rho$). Also, it is reasonable to use the channel opening ratio B_2/B_1 to account

for the combined effect of B_1 and B_2. In addition, the influence of kinematic viscosity v of water is insignificant for a turbulent flow over rough sediment beds (Yalin 1977). Therefore, applying these considerations, the Buckingham Π theorem (see Sect. 11.2.3) is used with U_{1e} and h_1 as repeating variables to obtain the following nondimensional equation:

$$\frac{d_s}{h_1} = f\left(F_{1e}, \frac{d_{50}}{h_1}, \frac{B_2}{B_1}\right) \tag{10.23}$$

where F_{1e} is the excess approaching flow Froude number $[= U_{1e}/(\Delta g h_1)^{0.5}]$. The condition $U_1 \rightarrow U_{cr}$ (that is the limiting condition for a clear-water scour, as $U_1 > U_{cr}$ corresponds to a live-bed scour) is recognized to be the most idealized condition for maximum equilibrium scour depth $[d_s]_{max}(= d_s|_{U_1=U_{cr}})$ in long contractions under a clear-water scour condition (Gill 1981). Therefore, to determine the equation of maximum equilibrium scour depth $[d_s]_{max}$ in long contractions, Eq. (10.23) is written for $U_1 \rightarrow U_{cr}$. Using the experimental data for clear-water scour, Dey and Raikar (2005) obtained the empirical equation of maximum equilibrium scour depth as follows:

$$\frac{[d_s]_{max}}{h_1} = 0.368 F_{1ec}^{0.55}\left(\frac{B_2}{B_1}\right)^{-1.26}\left(\frac{d_{50}}{h_1}\right)^{-0.19} \tag{10.24}$$

where $F_{1ec} = U_{1ec}/(\Delta g h_1)^{0.5}$ and $U_{1ec} = U_{cr} - U_1|_{U_2=U_{cr}}^{d_s=0}$. Equation (10.24) is written for uniform sediments, as it does not include σ_g.

The equilibrium scour depth $d_s(\sigma_g)$ in nonuniform sediments can be estimated in terms of geometric standard deviation σ_g of sediments using the following relationship:

$$d_s(\sigma_g) = K_\sigma d_s \tag{10.25}$$

where K_σ is the coefficient due to sediment gradation. The coefficient K_σ is defined as the ratio of equilibrium scour depth in nonuniform sediment ($\sigma_g > 1.4$) to that in uniform sediment. The variation of K_σ with σ_g is shown in Fig. 10.3 (Dey and Raikar 2005).

10.2.4 Other Scour Depth Predictors

Phenomena involving scour in long contractions have been studied extensively in laboratories, from which a number of semianalytical and empirical equations have been developed to estimate the equilibrium scour depth under both clear-water and live-bed scour conditions. In general, they are based on a limited range of data. Table 10.1 furnishes the empirical equations of equilibrium scour depth proposed by different investigators.

Fig. 10.3 Variation of K_σ as a function of σ_g (Dey and Raikar 2005)
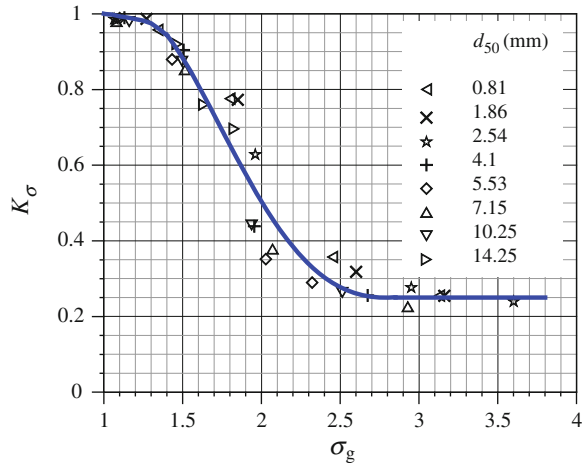
Table 10.1 Equations of equilibrium scour depth within channel contractions proposed by different investigators

References	Formula	Regime
Straub (1934)	$$\frac{d_s}{h_1} = \left(\frac{B_2}{B_1}\right)^{-6/7} \left\{ \left[\left(\frac{\tau_{0c}}{2\tau_{01}}\right)^2 + \left(\frac{B_2}{B_1}\right)^{-1} \right. \right.$$ $$\left. \left. \times \left(1 - \frac{\tau_{0c}}{\tau_{01}}\right) \right]^{0.5} + \frac{\tau_{0c}}{2\tau_{01}} \right\}^{-3/7} - 1$$	Clear-water
Komura (1966)	$$\frac{d_s}{h_1} = 1.6 Fr_1^{0.2} \left(\frac{B_2}{B_1}\right)^{-0.67} \sigma_g^{-0.5} - 1$$	Clear-water
	$$\frac{d_s}{h_1} = 1.45 Fr_1^{0.2} \left(\frac{B_2}{B_1}\right)^{-0.67} \sigma_g^{-0.2} - 1$$	Live bed
Gill (1981)	$$\frac{d_s}{h_1} = \left(\frac{B_2}{B_1}\right)^{-6/7} \left(\frac{\tau_{0c}}{\tau_{01}}\right)^{-3/7} - 1$$	Clear-water
	$$\frac{d_s}{h_1} = \left(\frac{B_2}{B_1}\right)^{-6/7} \left[\left(\frac{B_2}{B_1}\right)^{-1/m} \left(1 - \frac{\tau_{0c}}{\tau_{01}}\right) + \frac{\tau_{0c}}{\tau_{01}} \right]^{-3/7} - 1$$ where m is an exponent varying from 1.5 to 3	Live bed
Lim (1993)	$$\frac{d_s}{h_1} = 1.854 F_{1d}^{0.75} \left(\frac{B_2}{B_1}\right)^{-0.75} \left(\frac{d_{50}}{h_1}\right)^{0.25} - 1$$ where $F_{1d} = U_1/(\Delta g d_{50})^{0.5}$	Clear-water/live bed
Lim and Cheng (1998)	$$\frac{d_s}{h_1} = \left(\frac{B_2}{B_1}\right)^{-0.75} - 1$$	Clear-water/live bed

Note In order to obtain maximum equilibrium scour depth $[d_s]_{max}$, equations of d_s are to be expressed for the threshold condition $U_1/U_{cr} \to 1$ or $\tau_{01}/\tau_{01c} \to 1$. For uniform sediments ($\sigma_g < 1.4$), the geometric standard deviation σ_g is considered to be unity

10.3 Scour Downstream of Structures

10.3.1 Scour Below Drop Structures

Drops are provided in rivers for lowering the bed level when the slope of the river is smaller than the natural ground slope. These structures therefore artificially increase the slope of the rivers. The stream flow running over the drops is called an *overfall*. In addition, the scour is developed downstream of the bed protection provided to control the slope or elevation of the riverbed to create a drop. The water released from the drop structures impinges on the free surface of the tailwater as a jet, which is called *plunging jet*. This freely falling jet may have considerable potential to scour the bed downstream of the structures, and such scour is known as *jet scour*. Scour due to jets occurs very rapidly, which causes danger to the stability of the channel bed, in addition to the devastating effects on the hydraulic structures. Considerable portion of the energy of the flowing stream is dissipated through turbulent mixing in the pool due to plunging jet. Figures 10.4a, b show schematic of scour below weir type and free overfall type drop structures.

The pioneering study on scour below a drop structure was due to Schoklitsch (1932). He proposed the following empirical relationship for the equilibrium scour depth for the flow over structures:

$$d_s = K_0 \frac{q^{0.57} H^{0.2}}{d_{90}^{0.32}} - h_t \quad \wedge \quad \begin{cases} d_{90} \text{ in mm}, K_0 = 4.75 \text{ (in s}^{0.6} \text{ m}^{0.3}) \\ d_{90} \text{ in m}, K_0 = 0.52 \text{ (in s}^{0.6} \text{ m}^{0.3}) \end{cases} \quad (10.26)$$

where q is discharge per unit width, H is the height between upstream and downstream water levels, d_{90} is the 90 % finer sediment size, and h_t is the tailwater depth.

Based on the dimensional analysis and using the experimental data, Kotoulas (1967) developed a relationship for the equilibrium scour depth downstream of a structure. It is

$$d_s = \frac{1.9}{g^{0.35}} \cdot \frac{q^{0.7} H^{0.35}}{d_{95}^{0.4}} - h_t \quad (10.27)$$

where d_{95} is the 95 % finer sediment size.

For free overfall type drop structures, Dey and Raikar (2007b) proposed a procedure to calculate the jet velocity U_0 and the jet thickness l_0 at the entry of jet into the tailwater.[1]

---

[1] Dey and Raikar (2007b) considered section 0 at the upstream of the drop where the critical depth h_c occurs and section 0 at the entry of jet into the tailwater (Fig. 10.4b). The continuity equation applied between sections 1 and 0 is

Fahlbusch ([1994](#)) proposed an empirical equation of equilibrium scour depth for weir type drop structures. He expressed scour depth d_s as a function of q and jet velocity U_0 entering the tailwater depth h_t at an angle θ_j with the horizontal at the water level as

$$d_s = K_p \left(\frac{qU_0}{g} \sin \theta_j \right)^{0.5} - h_t \tag{10.28}$$

The coefficient K_p is dependent on sediment size. For gravel, $3 < K_p < 5$; for sand, $5 < K_p < 20$; and for silt, $K_p \approx 20$.

Later, a more generalized relationship of equilibrium scour depth for weir type drop structures was recommended (Graf [1998](#)). It is

$$d_s = \frac{3.6}{\Delta^{4/9} g^{0.3}} \cdot \frac{q^{0.6} H^{0.5}}{d_{90}^{0.4}} - h_t \tag{10.29}$$

Also, D'Agostino and Ferro ([2004](#)) suggested a simplified equation of equilibrium scour depth for weir type drop structures as

$$\frac{d_s}{Z} = 0.975 \left(\frac{h}{Z} \right)^{0.863} \tag{10.30}$$

(Footnote 1 continued)

$$U_c h_c = U_0 l_0$$

where U_c is the critical velocity of the flow upstream of the drop. According to Bakhmeteff ([1932](#)), the jet velocity U_0 is given by

$$U_0 = C_0 [2g(h_0 + 1.5h_c)]^{0.5}$$

where C_0 is the velocity coefficient and h_0 is the height of drop above the tailwater level.
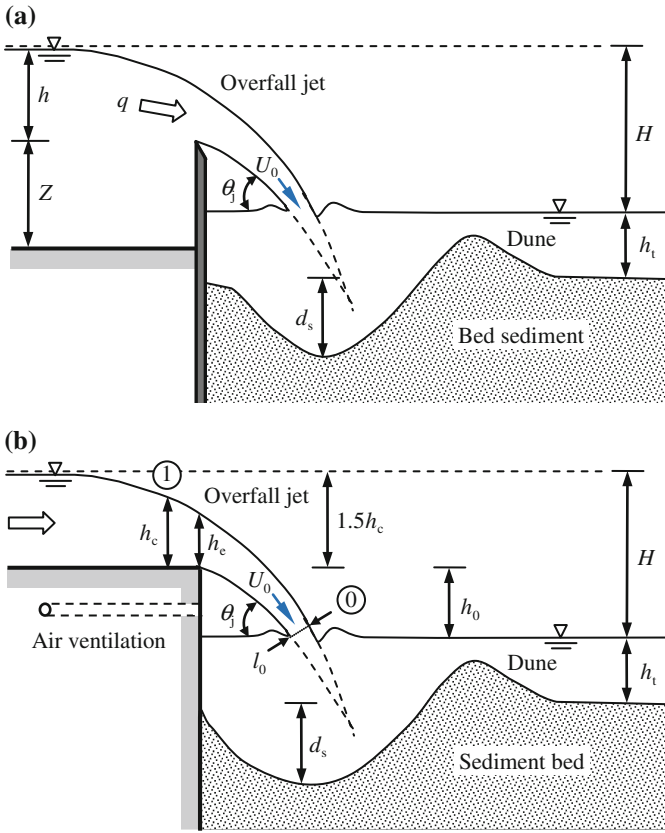
Using the value of end-depth-ratio ($= h_e/h_c$, where h_e is the end depth) for rectangular channels equaling 0.715 as given by Rouse ([1936](#)), the above equation becomes

$$U_0 = C_0 [2g(h_0 + 2.1h_e)]^{0.5}$$

Inserting into the continuity equation, the expression for jet thickness l_0 can be written as

$$l_0 = \frac{1.17 h_e^{1.5}}{C_0 (h_0 + 2.1h_e)^{0.5}}$$

Using the experimental data, the value of C_0 was estimated as 0.672.

Fig. 10.4 Schematic of scour below drop structures: **a** weir type and **b** free overfall type

where Z is the crest height of the weir and h is the flow depth over a weir (Fig. 10.4a). Note that Eq. (10.30) does not take into account the effects of sediment size and tailwater depth.

Stein et al. (1993) developed an analytical equation to predict the equilibrium scour depth downstream of a headcut type drop structure for the condition of shallow tailwater depth ($d_s \gg h_t$) (Fig. 10.5). Neglecting the effects of tailwater depth, they proposed

$$d_s = \frac{C_d^2 \lambda_f \rho U_0^2 l_0}{\tau_{0c}} \sin \theta_j \quad \wedge \quad \lambda_f = 0.0275 \left(\frac{\upsilon}{q} \right)^{0.25} \quad (10.31)$$

where C_d is the jet diffusion coefficient (= 2.6).
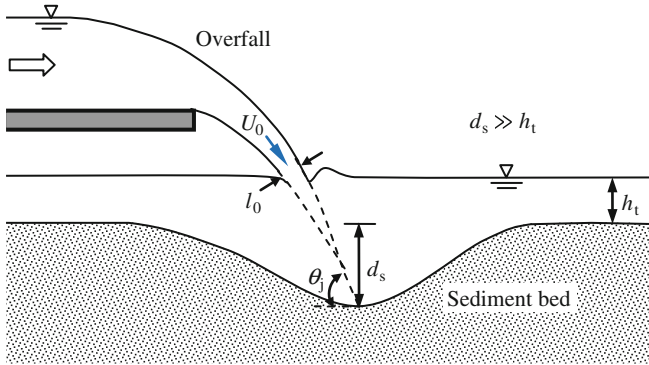
Fig. 10.5 Schematic of scour below a headcut

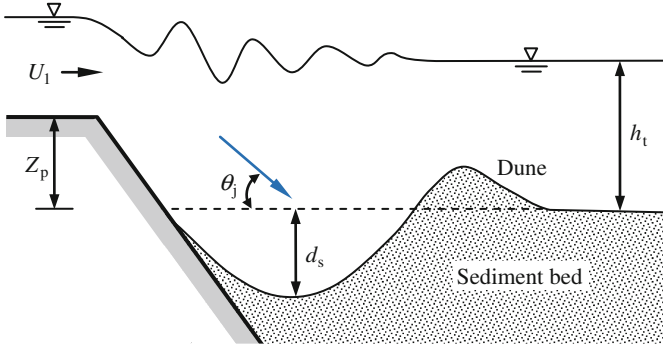## 10.3.2 Scour Downstream of Grade-Control Structures

Grade-control structures are employed to prevent excessive riverbed degradation (Fig. 10.6). Bormann and Julien (1991) investigated the scour downstream of grade-control structures based on two-dimensional jet diffusion and particle stability. They put forward the following expression for the equilibrium scour depth:

$$d_s = \left\{ 1.8 \left[\frac{\sin \phi}{\sin(\phi + \theta_j)} \right]^{0.8} \frac{q^{0.6} U_1 \sin \theta_j}{(\Delta g)^{0.8} d_{90}^{0.4}} \right\} - Z_p \qquad (10.32)$$

where U_1 is the approaching velocity, Z_p is the drop height of grade-control structure, θ_j is the jet angle near the original bed level, and ϕ is the angle of repose of bed sediment.

10.3.3 Scour Downstream of Bed Sills

Mountain streams are frequently subjected to channel incision. One of the methods to stabilize them is to employ a series of transverse structures called *bed sills*. Bed sills are generally preferred when the height of the riverbed is to be somewhat raised in order to reduce instability of the valley slope. The overfall plunging jet issued from a sill crest diffuses its energy in mixing process through rollers inside the downstream pool below. Further downstream, a uniform flow can be established if the riverbed has an equilibrium slope for a significant length. This condition is satisfied when the intermediate distance between two bed sills is adequately long. Flow over immediate upstream of a sill crest is characterized by a critical flow condition. At the edge of the sill, the flow becomes supercritical, being accelerated by that gravity as an overfall jet that has significant power to

Fig. 10.6 Schematic of scour downstream of a grade-control structure

remove sediment from the bed downstream of a bed sill. Practically, scour downstream of a bed sill endangers its stability leading to the failure if the maximum scour depth is deep enough to expose the foundation (Fig. 10.7).

According to Gaudio et al. (2000), the maximum clear-water scour depth d_s at a bed sill can be given as a functional form. It is

$$d_s = d_s(g, \, v, \, \rho, \Delta\rho, \, q, \, h_1, \, d_{50}, \, a_1) \qquad (10.33)$$

where h_1 is the uniform flow depth and a_1 is the morphological drop which is defined by

$$a_1 = (S_0 - S_{eq})L \qquad (10.34)$$

where S_0 is the initial streamwise bed slope, S_{eq} is the equilibrium bed slope, and L is the distance between two neighboring sills. The equilibrium slope in clear-water condition can be expressed by the threshold Shields parameter Θ_c for the initiation of bed particle motion under fully developed turbulence flow condition. It is

$$\Theta_c = \frac{h_1 S_{eq}}{\Delta d_{50}} = \text{constant} \qquad (10.35)$$

From the Manning equation, one can write

$$q = \frac{h_1^{5/3} S_{eq}^{0.5}}{n} \qquad (10.36)$$

where n is the Manning roughness coefficient. Using Eqs. (10.35) and (10.36), the uniform flow depth and the equilibrium bed slope can be obtained as
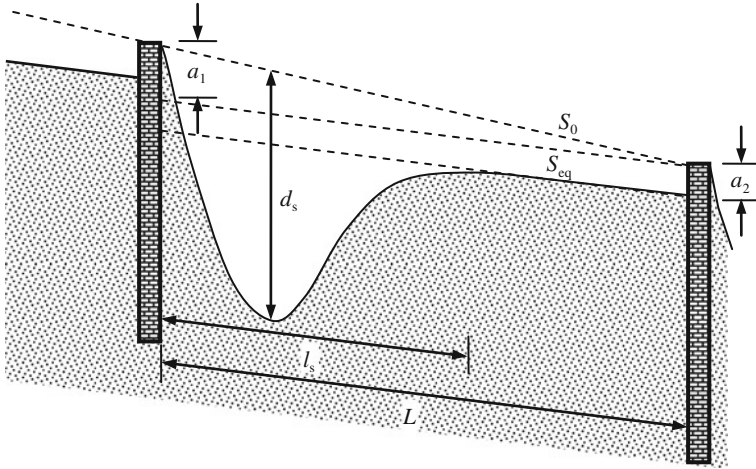
Fig. 10.7 Definition sketch of scour at a bed sill (Gaudio et al. 2000; Lenzi et al. 2002)

$$h_1 = \frac{(nq)^{6/7}}{(\Theta_c \Delta d_{50})^{3/7}} \tag{10.37a}$$

$$S_{eq} = \frac{(\Theta_c \Delta d_{50})^{10/7}}{(nq)^{6/7}} \tag{10.37b}$$

Equation (10.37a) provides the dependency of the uniform flow depth on other flow and sediment parameters. This allows h_1 to be dropped from Eq. (10.33).

The specific energy E_s on the sill is given by

$$E_s = 1.5 \left(\frac{q^2}{g}\right)^{1/3} \tag{10.38}$$

Applying Buckingham Π theorem (see Sect. 11.2.3) to Eq. (10.33) devoid of h_1, one can write

$$\frac{d_s}{E_s} = f\left(\frac{q}{\upsilon}, \Delta, \frac{a_1}{\Delta d_{50}}, \frac{a_1}{E_s}\right) \tag{10.39}$$

For fully developed turbulent flow, kinematic viscosity υ can be neglected. Further, Δ is assumed to be a constant. Equation (10.39) thus reduces to

$$\frac{d_s}{E_s} = f\left(\frac{a_1}{\Delta d_{50}}, \frac{a_1}{E_s}\right) \tag{10.40}$$

Experiments by Gaudio and Marion (2003) revealed that only the first nondimensional parameter of the right-hand side of Eq. (10.40) influences the scour depth. The empirical equation of scour depth given by Gaudio and Marion is

$$\frac{d_\mathrm{s}}{E_\mathrm{s}} = 0.18\,\frac{a_1}{\Delta d_{50}} + 0.369 \tag{10.41}$$

The above equation is applicable for $1.3 \leq a_1/(\Delta d_{50}) \leq 9.1$. The length of the scour hole is as follows (Gaudio et al. 2000):

$$\frac{l_\mathrm{s}}{E_\mathrm{s}} = 1.87\,\frac{a_1}{\Delta d_{50}} + 4.02 \tag{10.42}$$

Later, Lenzi et al. (2002) recognized that both the nondimensional parameters of the right-hand side of Eq. (10.40) affect the scour depth. They put forward expressions for the scour depth and the length of the scour hole as

$$\frac{d_\mathrm{s}}{E_\mathrm{s}} = 0.436 + 1.453\left(\frac{a_1}{E_\mathrm{s}}\right)^{0.863} + 0.06\left(\frac{a_1}{\Delta d_{95}}\right)^{1.491} \tag{10.43a}$$

$$\frac{l_\mathrm{s}}{E_\mathrm{s}} = 4.479 + 0.023\left(\frac{a_1}{E_\mathrm{s}}\right)^{-1.81} + 2.524\left(\frac{a_1}{\Delta d_{95}}\right)^{1.13} \tag{10.43b}$$

10.3.4 Scour Due to Horizontal Jets Issuing from a Gate Opening

The scour phenomenon downstream of a sluice gate opening is complex in nature owing to the abrupt change of the flow characteristics on the sediment bed (Dey and Sarkar 2006a) (Fig. 10.8). Scour initiates at the downstream edge of the apron when the bed shear stress exerted by the submerged jet exceeds the threshold bed shear stress for the bed sediment. In the initial stage, the evolution of the vertical dimension of scour hole is faster than the longitudinal one, and the suspended load is the only mode of sediment transport. However, with the development of the vertical dimension of the scour hole, the mode of sediment transport changes to a combination of suspended load and bed load. As the flow separation takes place at the edge of the apron having a reattachment of flow at the deepest point of the scour hole, the movement of the sediment particles is divided into two parts. Some amount of sediments move along the downstream slope of the scour hole and ultimately go out of the scour hole. The other part moves back toward the upstream along the upstream slope of the scour hole by the reversed flow. The upstream portion of the scour hole achieves a steep slope.
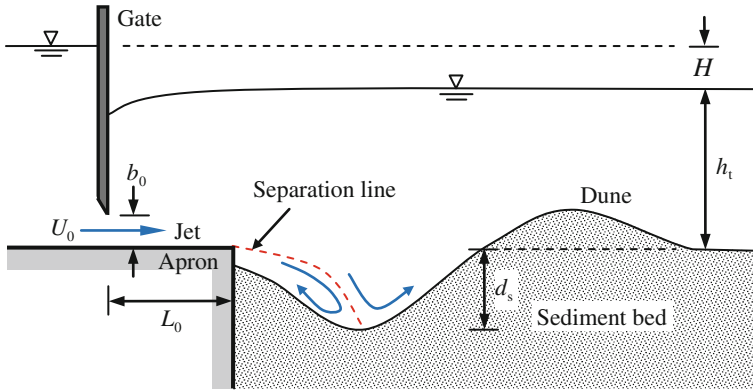
Fig. 10.8 Schematic of scour due to horizontal jet issuing from a sluice gate opening

The theory of submerged plane wall jet was developed by Dey et al. (2010). They derived the velocity and Reynolds stress distributions in submerged wall jets (see Sect. 10.8.1). The theory would help the future researchers to model scour downstream of an apron due to submerged wall jets. However, Dey and Sarkar (2006b) gave a semiempirical model of the same. The application of the theory of submerged wall jet to compute scour is discussed in Sect. 10.8.2.

Qayoum (1960) studied the scour downstream of a vertical gate without apron ($L_0 = 0$). Using the dimensional analysis, he proposed an empirical equation

$$d_s = \frac{2.78}{g^{0.2}} \cdot \frac{q^{0.4} H^{0.22} h_t^{0.4}}{d_{90}^{0.22}} - h_t \tag{10.44}$$

Altinbilek and Basmaci (1973) proposed an equation of scour depth due to submerged jets issuing from a sluice opening as

$$d_s = b_0 \left(\frac{b_0}{d_{50}} \tan\phi \right)^{0.5} \left[\frac{U_0}{(\Delta g b_0)^{0.5}} \right]^{1.5} \tag{10.45}$$

where b_0 is the thickness of sluice opening and U_0 is the issuing velocity of jet.

Breusers and Raudkivi (1991) gave

$$d_s = 8 \times 10^{-3} b_0 \left(\frac{U_0}{u_{*c}} \right)^2 \tag{10.46}$$

Hoffmans (1998) [also Hoffmans and Verheij (1997)] derived equilibrium scour depth due to submerged jets (with $L_0 = 0$) by applying the momentum principle between the vertical section at the sluice opening and the section passing through the dune crest as

$$d_s = b_0 \frac{50}{\lambda_s} \left(1 - \frac{U_{crest}}{U_0} \right) \tag{10.47}$$

where λ_s is the scour factor dependent on d_{90}, and U_{crest} is the average velocity over the downstream dune crest. The values of λ_s are $\lambda_s(d_{90} = 0.1 \text{ mm}) = 1.4$, $\lambda_s(d_{90} = 0.3 \text{ mm}) = 2$, $\lambda_s(d_{90} = 0.5 \text{ mm}) = 2.3$, $\lambda_s(d_{90} = 1 \text{ mm}) = 2.95$, $\lambda_s(d_{90} = 3 \text{ mm}) = 4.3$, $\lambda_s(d_{90} = 5 \text{ mm}) = 5.1$, $\lambda_s(d_{90} = 10 \text{ mm}) = 6.3$, and $\lambda_s(d_{90} \geq 12 \text{ mm}) = 6.8$.

Shalash (1959) and Dey and Sarkar (2006a) conducted experiments and proposed empirical equations of equilibrium scour depth downstream of an apron due to submerged jets issuing from a sluice opening. According to Shalash (1959),

$$d_s = 0.61 \frac{q^{0.6}(H + h_t)^{0.5}}{d_{90}^{0.4}} \left(1.5 \frac{H}{L_0} \right)^{0.6} - h_t \tag{10.48}$$

and according to Dey and Sarkar (2006a),

$$d_s = 2.59 b_0 \left[\frac{U_0}{(\Delta g d_{50})^{0.5}} \right]^{0.94} \left(\frac{b_0}{L_0} \right)^{0.37} \left(\frac{h_t}{b_0} \right)^{0.16} \left(\frac{d_{50}}{b_0} \right)^{0.25} \tag{10.49}$$

Eggenberger and Müller (1944) investigated scour downstream of hydraulic structures due to a combined overfall and submerged jet (Fig. 10.9). They gave a general relationship for equilibrium scour depth as

$$d_s = \frac{c_0}{15.849} \cdot \frac{q^{0.6} H^{0.5}}{d_{90}^{0.4}} - h_t \quad \wedge \quad c_0 = 22.88 - 10^3 (4.9\hat{q}^3 - 6.3\hat{q}^2 + 29\hat{q} + 64)^{-1} \tag{10.50}$$

where $\hat{q} = q_1/q_0$, q_1 is the overfall discharge per unit width, and q_0 is the submerged jet discharge per unit width through a sluice opening. By definition of continuity, total discharge per unit width is $q = q_1 + q_0$. For overfall only, c_0 ($\hat{q} \gg 1$) = 22.88 $s^{0.6}$ $m^{-0.3}$; and for submerged jets only, c_0 ($\hat{q} \ll 1$) = 10.35 $s^{0.6}$ $m^{-0.3}$.

10.4 Scour Below Horizontal Pipelines

Local scour below pipelines, laid on and across the riverbeds to convey water, oil, gas, or any fluid, commonly occurs by the erosive action of flowing stream. Scour may leave a pipeline unsupported over a considerable distance resulting in fatigue failure due to flow-induced oscillation by wake vortex shedding. Therefore, one of
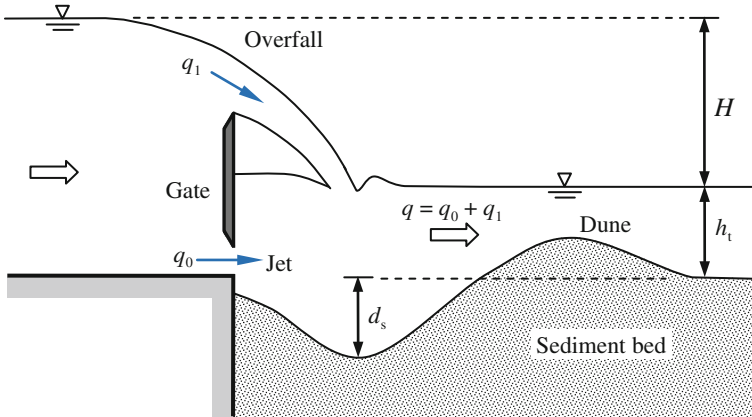
Fig. 10.9 Schematic of scour due to a combined action of overfall and submerged jet allowed by a sluice gate

the imperative aspects of pipeline design is to predict the magnitude of scour below pipelines.

When a pipeline is laid on an erodible bed with a little embedment e (Fig. 10.10), it is subjected to a hydrodynamic force, and a pressure gradient is set up between the two sides of the pipeline. At the same time, the pressure gradient between upstream and downstream contact points (A and B) is also set up in the sediment bed immediately below the pipeline. Due to this pressure gradient, the subsurface seepage flow is driven below the pipeline. As the flow velocity increases, the pressure gradient is simultaneously enhanced, because the pressure intensity is proportional to the quadratic of the flow velocity. With an increase in pressure gradient dp/dx (where p is the pressure intensity and x is the distance along the pipe perimeter), a condition is reached when the sediment below the pipeline starts to dislodge and is called *scour threshold*. The mechanism of scour below a pipeline under a steady flow is described as follows (Sumer and Fredsøe 2002):

Once a threshold point is reached, the seepage flux increases rapidly than the order of the pressure gradient by which the seepage is driven. At the same time, the surface of the sediment bed in the immediate downstream of the pipeline bulges. Eventually, the sediment–water mixture breaks through the space underneath the pipeline, which is called *piping* (Fig. 10.11). Sumer and Fredsøe (2002) derived the threshold condition of piping through a simple calculation by balancing the upward seepage pressure force and the submerged weight of sediment at the exit point B (see Fig. 10.10). It is

$$\frac{1}{\rho g} \cdot \frac{\mathrm{d}p}{\mathrm{d}x} \geq \Delta(1 - \rho_0)$$

Fig. 10.10 Schematic of seepage flow induced below a pipeline
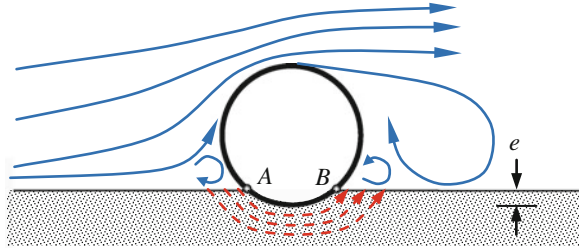
Fig. 10.11 Piping
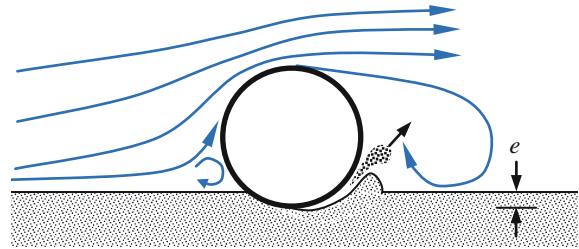
where ρ_0 is the porosity of the sediment. Further, Sumer et al. (2001) determined the threshold condition empirically in terms of velocity considering a small embedment e of the pipeline having an external diameter D. Using the above relationship and the laboratory experimental data, they proposed

$$\frac{U_{gcr}^2}{\Delta g(1 - \rho_0)D} = 0.025 \exp\left(81\frac{e}{D}\right)^{0.5} \qquad (10.51)$$

where U_{gcr} is the threshold velocity of scour below a pipeline. Note that the scour does not initiate all along the length of the pipeline simultaneously, but occurs locally.

After the piping process, a small gap is developed between the pipeline and the bed. A considerable magnitude of flow is diverted to the gap leading to a flow concentration in the gap. It enhances the shear stress acting on the bed immediately below the pipeline. The enhanced bed shear stress is of the order of magnitude of three times the bed shear stress of the approaching flow (Jensen et al. 1990). As a result, a large amount of sediment is scoured underneath the pipeline. The sediment–water mixture is spouted from the enlarged gap. Such scour process is known as *tunnel erosion* (Fig. 10.12). With an increase in gap size, the gap velocity decreases and the tunnel erosion gradually seizes. This stage is followed by *lee-wake erosion*.

As a result of tunnel erosion, a dune is formed on the downstream end of the pipeline and it gradually migrates further downstream. Finally, the dune disappears as the scour progresses. At this stage, the scour is governed by the *lee-wake*

Fig. 10.12 Tunnel erosion
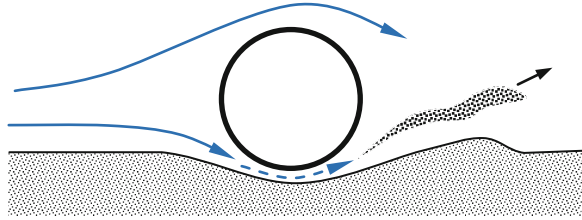
Fig. 10.13 Lee-wake erosion
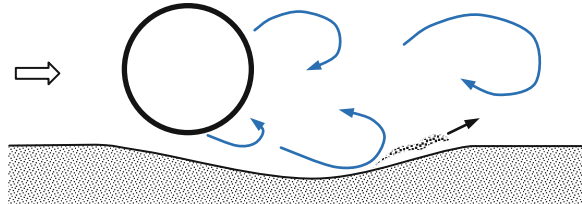
erosion, which occurs due to the vortex shedding on the downstream end of the pipeline (Fig. 10.13). At the end of the tunnel erosion, when the gap between the pipeline and the bed enlarges to a certain magnitude, the vortex shedding begins. The vortices that shed from the pipe wall sweep the sediment as they get convected downstream. During this period, the bed shear stress increases by about four times having a greater scour potential at the lee end of the pipe. However, the bed shear stress gradually reduces with the enlargement of the scour hole size. The equilibrium is reached when the bed shear stress underneath the pipeline reaches the value being equal to the threshold bed shear stress for sediment motion in clearwater case or equal to the approaching bed shear stress in live-bed case. Figure 10.14 shows the photograph of an equilibrium scour below a pipe in a flume.

10.4.1 Estimation of Gap Discharge

In studying scour below a pipeline, estimation of gap discharge is an important aspect. It can be determined analytically as described here. The schematic of a scour hole below a pipeline and the coordinate system are shown in Fig. 10.15, where the origin of the coordinate system lies at the contact point of the circular pipe with the initial bed level. According to Chao and Hennessy (1972), the *image method* of potential flow theory is applicable assuming a steady flow around the pipeline and neglecting the curvature effect of the scour hole. The potential function ϕ and the stream function ψ governing the flow are

Fig. 10.14 Photograph of an equilibrium scour below a pipe in an experimental flume. Flow took place from the right to left
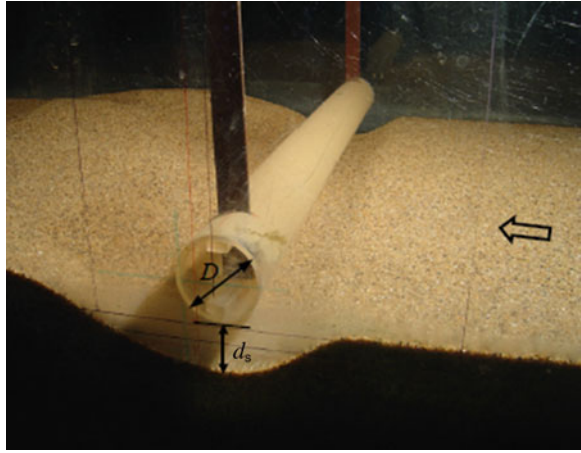
Fig. 10.15 Schematic of a scour hole below a pipeline and the coordinate system
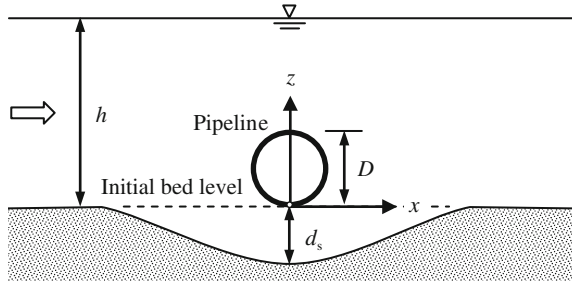
$$\phi = U_0 x \left\{ 1 + \frac{D^2}{4[x^2 + (z - 0.5D)^2]} + \frac{D^2}{4[x^2 + (z + 2d_s + 0.5D)^2]} \right\} \quad (10.52a)$$

$$\psi = U_0 (z + d_s) \left\{ 1 - \frac{D^2}{4[x^2 + (z - 0.5D)^2]} - \frac{D^2}{4[x^2 + (z + 2d_s + 0.5D)^2]} \right\}$$

$$(10.52b)$$

where U_0 is the depth-averaged velocity up to the elevation of the horizontal diameter of the pipeline, that is, $z = 0.5D$. It can be estimated assuming a logarithmic law of approaching velocity as $U_0 = 5.75u_* \log (2.765D/d_{50})$, where u_* is the approaching shear velocity. Here, it is intuitive that the flow through the gap is

contributed by the approaching flow velocity up to the elevation of the horizontal diameter of the pipeline from the bed level. Hence, the horizontal velocity component $\bar{u}$ within the scour hole is given by

$$\bar{u} = \frac{\partial \phi}{\partial x} = U_0 \left\{ 1 + \frac{D^2}{4[x^2 + (z - 0.5D)^2]} - \frac{x^2 D^2}{2[x^2 + (z - 0.5D)^2]^2} \right.$$
$$\left. + \frac{D^2}{4[x^2 + (z + 2d_s + 0.5D)^2]} - \frac{x^2 D^2}{2[x^2 + (z + 2d_s + 0.5D)^2]^2} \right\} \qquad (10.53)$$

Integrating $\bar{u}$ within limits $z = -d_s$ and $z = 0$, the gap discharge q_g is obtained as

$$q_g = \int_{-d_s}^{0} \bar{u} dz = U_0 \left[d_s + 0.5D - \frac{D^2}{4(2d_s + 0.5D)} \right] \qquad (10.54)$$

Alternatively, one can also estimate the gap discharge q_g from the graphical solution given by Chiew (1991) as h/D is a function of q_g/q, where h is the flow depth and q is the free stream discharge per unit width in the channel. However, it would be convenient to use his graphical solution if it is expressed as follows (Dey and Singh 2007):

$$q_g = 0.781 q \left(\frac{D}{h} \right)^{0.787} \qquad (10.55)$$

10.4.2   Scour Depth Estimation

Phenomena involved in local scour below underwater pipelines have been studied most extensively in the laboratory experiments, from which a number of empirical equations and the methodologies have been developed to estimate the equilibrium scour depth below pipelines. The important predictors of scour depth are summarized below:

Kjeldsen et al. (1973) were the pioneer to give an empirical relationship for equilibrium scour depth below pipelines. It is

$$d_s = 0.972 \left(\frac{U^2}{2g} \right)^{0.2} D^{0.8} \qquad (10.56)$$

The Dutch research group (Bijker and Leeuwestein 1984) put forward the following empirical equation of scour depth below an underwater pipeline:

$$d_s = 0.929 \left(\frac{U^2}{2g} \right)^{0.26} \frac{D^{0.78}}{d_{50}^{0.04}} \qquad (10.57)$$

The empirical equations proposed by Ibrahim and Nalluri (1986) for the estimation of scour depth below pipelines in clear-water and live-bed conditions are

$$\text{Clear-water scour:} \quad \frac{d_s}{D} = 4.706 \left(\frac{U}{U_{cr}} \right)^{0.89} Fr^{1.43} + 0.06 \qquad (10.58a)$$

$$\text{Live-bed scour:} \quad \frac{d_s}{D} = 0.084 \left(\frac{U}{U_{cr}} \right)^{-0.3} Fr^{-0.16} + 1.33 \qquad (10.58b)$$

where Fr is the Froude number [$= U/(gh)^{0.5}$] and U_{cr} is the threshold velocity for sediment motion.

Chiew (1991) proposed the following iterative method to predict equilibrium scour depth below pipelines:

1. For a given value of h/D, determine the gap discharge q_g.
2. Assume a scour depth d_s and estimate the average gap velocity U_g below the pipeline by $U_g = q_g/d_s$.
3. Compute the shear stress τ_0 on the scoured bed using $\tau_0 = \lambda_D \rho U_g^2 / 8$, where the friction factor λ_D can be estimated from the Moody diagram for a relative roughness ($= d_{50}/d_s$) and a Reynolds number ($= U_g d_s/\upsilon$).
4. Compare τ_0 with the threshold bed shear stress τ_{0c} obtained from the Shields diagram. Continue the iteration for different values of d_s until $\tau_{0c} = \tau_0$.

Moncada-M and Aguirre-Pe (1999) suggested the following empirical equation of equilibrium scour depth below an underwater pipeline:

$$\frac{d_s}{D} = 0.9 \tanh \left[1.4 \frac{U}{(gh)^{0.5}} \right] + 0.55 \qquad (10.59)$$

With consideration of an initial gap e between the original bed level and the pipe bottom above the bed level, Moncada-M and Aguirre-Pe (1999) proposed

$$\frac{d_s}{D} = 2Fr \, \text{sech} \left(1.7 \frac{e}{D} \right) \qquad (10.60)$$

Based on wall correction method (Sect. 3.9), Dey and Singh (2007) put forward a simplified iterative method for the computation of equilibrium scour depth. Dey and Singh (2008) conducted an extensive experimental study to explore the

Fig. 10.16 Influence of pipe Froude number F_D on scour depth d_s (Dey and Singh 2008)
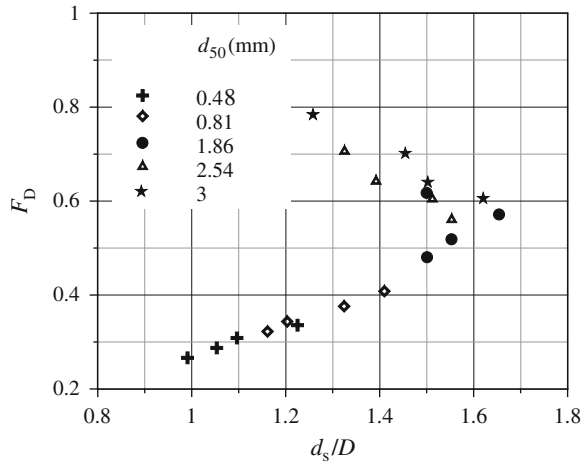
Fig. 10.17 Variation of K_σ as a function of σ_g (Dey and Singh 2008)
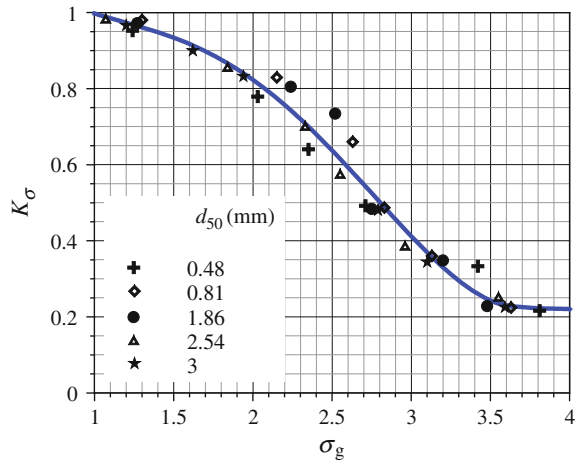
influence of various parameters on equilibrium scour depth in clear-water condition ($U/U_{cr} \approx 0.9$). The equilibrium scour depth d_s increases with an increase in approach flow depth h for shallow flow depths, becoming independent of higher flow depths when $h/D > 5$. The curve of scour depth versus pipe Froude number F_D [$= U/(\Delta gD)^{0.5}$] has a maximum value of $d_s/D = 1.65$ at $F_D = 0.58$ (Fig. 10.16).

Dey and Singh (2008) also studied the influence of sediment gradation on scour depth. The influence of sediment gradation was found to be prominent for non-uniform sediments, which reduce scour depth to a large extent due to the formation of armor layer within the scour hole. The variation of K_σ with σ_g is shown in Fig. 10.17. Further, the influence of different shaped cross sections of pipes on the

scour depth was investigated, where the *shape factors*[2] for circular, 45° (diagonal facing), and 90° (side facing) square pipes were obtained as 1, 1.29, and 1.91, respectively.

10.5 Scour at Bridge Piers

At bridge sites, localized scour in the vicinity of piers, over which the bridge superstructure rests, poses a challenging problem to the hydraulic engineers. Figure 10.18 shows the photograph of bridge piers, where the scour takes place even in the summer season at a lean flow discharge condition. Failure of bridges due to scour at pier foundations is a common occurrence, if the magnitude of scour is too large to uncover the pier foundations. The obstruction to the approaching flowing stream by a bridge pier causes a three-dimensional separation of flow forming a vortex flow and a periodical vortex shedding downstream of the pier. The complexity in flow structure increases with the development of the scour hole. To be more explicit, the flow separates at the upstream face of the pier as it travels by the side of the pier, creating a vortex trail, termed *horseshoe vortex*. The vortex moves downstream and as a result of which local scour takes place around the pier due to the removal of bed sediment. The scour at bridge piers has been studied extensively by various researchers. Reviews of the important experiments and field studies were given by Breusers et al. (1977), Dey (1997a, b), Melville and Coleman (2000), and Richardson and Davis (2001). Figure 10.19 shows the photograph of an equilibrium scour hole at a circular pier in an experimental flume. It gives an idea about the shape of the scour hole that occurs at a pier.

According to Raudkivi (1986), the approaching flow, which is stationary at the upstream face of the pier, is maximum at the free surface and decreases to zero at the bed in the free flow (unobstructed by the pier) reach. The stagnation pressure at the upstream face of the pier decreases in the downward direction causing the flow to be driven down along the face of the pier, producing a *downflow*. The downflow along the vertical plane of symmetry of the pier has a velocity profile with zero at the pier wall and again at some distance upstream of it. The maximum magnitude of downflow, at any elevation in the upstream, measured by Ettema (1980) occurs at 0.02–$0.05b$ from the pier face being closer to the pier lower down. Here, b is the pier width across the flow (or pier diameter in case of a circular pier). The *horseshoe vortex* developed due to the flow separation at the upstream edge of the scour hole rolls to form a helical flow, which is similar to the ground roller downstream (leeside) of a dune crest (see Sect. 8.2.2). It migrates downstream by the side of the pier for a few pier diameters before losing its existence becoming a

---

[2] *Shape factor* is the ratio of the equilibrium scour depth for a given non-circular pipe to that for a circular shaped pipe having a same diameter to the vertical cross-sectional length of the non-circular pipe.

Fig. 10.18 Scour taking place at bridge piers in a field condition. Photograph by the author
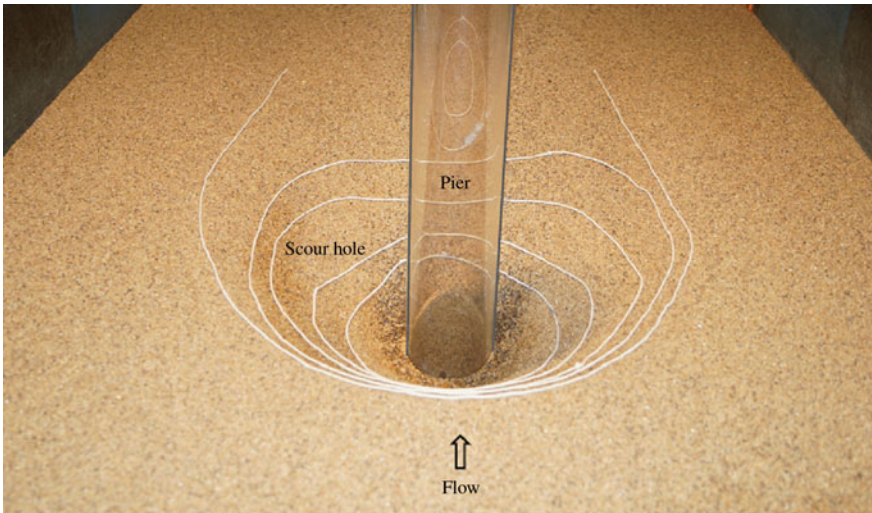
Fig. 10.19 Photograph of an equilibrium scour at a circular pier in an experimental flume

part of the general turbulence. The horseshoe vortex is a consequence of scour, not the cause of scouring. It also pushes the downflow inside the scour hole closer to the pier. The *bow wave*, formed at the free surface adjacent to the pier face rotating in a direction opposite to that of the horseshoe vortex, becomes pertinent in relatively shallow flows where it can interfere with the approaching flow causing a reduction in downflow velocity. The stagnation pressure also accelerates the flow by the side of the pier, resulting in a flow separation at the side and creating a *wake* with the cast-off vortices at the interfaces to the main flow. The cast-off vortices travel downstream with the flow and interact with the horseshoe vortex at the bed

(a)

(b)
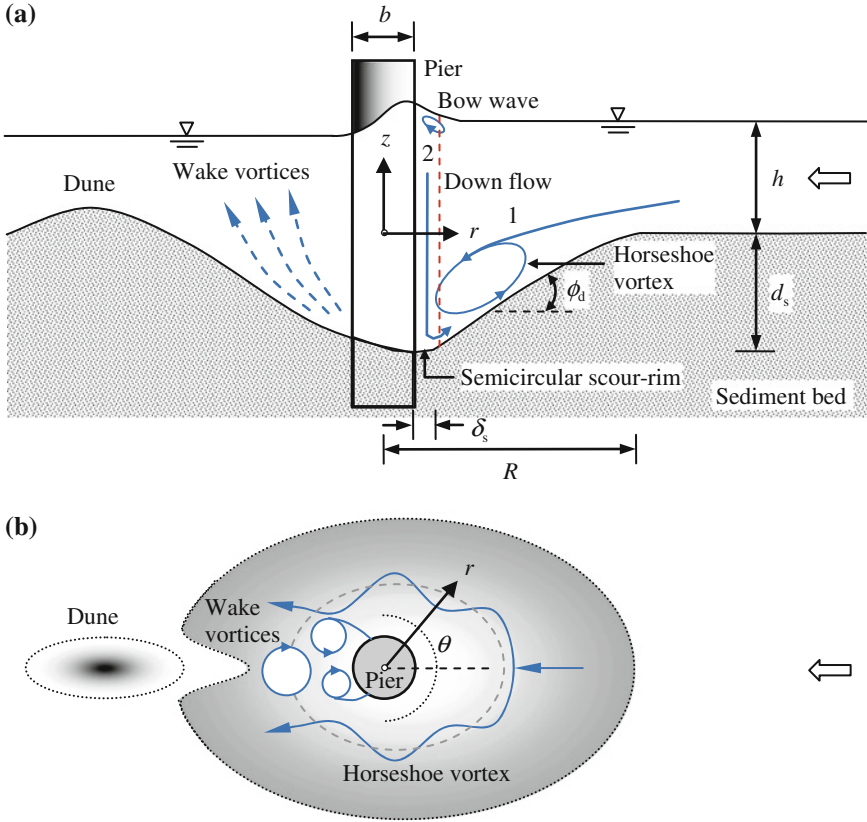
Fig. 10.20 Typical geometry of a scour hole and the components of flow field at a circular pier: **a** *elevation view* and **b** *plan view*

causing it to oscillate. Figures 10.20a, b show the typical geometry of a scour hole and the components of the flow field at a pier.

Conducting an experimental study, Dey (1991) described the clear-water scouring process at a circular pier. According to him, the horseshoe vortex is formed due to the diving mode of approaching flow into the scour hole. In the upstream of a pier, the sediment particles are mainly dislodged by the action of the downflow and subsequently pulled up along the upstream slope of the scour hole by the upward velocity of the horseshoe vortex. The scour hole is also fed by the sediment due to the collapse of the slant bed of scour hole, and finally, the sediment particles are drifted downstream by the arms of the horseshoe vortex along the circumference of the pier. The process of digging by the downflow along with the slant bed erosion continues until a quasi-equilibrium state is reached (Dey 1995). In this state, the scour hole is continually fed by a small amount of sediment particles due to slant bed erosion without a noticeable change in scour depth. The equilibrium, when the erosion ceases, is reached after a long period of time.

In quasi-equilibrium state, the average upstream slope of the scour hole, termed *dynamic angle of repose* ϕ_d, is about 10–20 % greater than the angle of repose ϕ of sediment in still water. A flat semicircular rim is formed around the upstream pier base (Fig. 10.20a). On downstream, the scour initiates at the pier base due to wake vortices (which act like a tornado) in the form of a spontaneous lifting of sediment particles by the action of suction from the each core of wake vortices. In the further downstream, a dune is progressively formed by the substantial deposition of sediment and side scouring. The dune, thus formed, slowly migrates downstream with the development of the scour hole. The erosion continues on both sides of the dune to form a shallow channel on either side having an adverse longitudinal slope that is flatter than the upstream slope.

Melville (1975), Dey et al. (1995), Dey (1995), Graf and Istiarto (2002) and Dey and Raikar (2007a) and Raikar and Dey (2008) measured the flow field in a scour hole at a pier. The flow measurement was done by hot-wire anemometry (Melville 1975), five-hole pitot sphere (Dey et al. 1995), and acoustic Doppler velocity profiler (Graf and Istiarto 2002). On the other hand, Dey and Raikar (2007a) and Raikar and Dey (2008) measured the flow by an acoustic Doppler velocimeter (ADV) and studied the characteristics of turbulent horseshoe vortex flow within the developing scour hole at cylindrical piers. Figure 10.21 shows the time-averaged velocity vectors at the upstream axis of symmetry of a pier in an equilibrium scour hole. The horseshoe vortex flow is well evident within the scour hole.
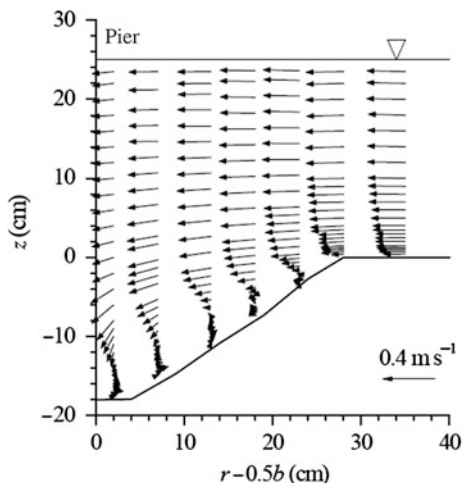
10.5.1 Kinematic Model of Horseshoe Vortex

Dey et al. (1995) developed a kinematic model for the horseshoe vortex flow in a scour hole at a pier.

In the upstream, the azimuthal section of a quasi-equilibrium scour hole, as shown in Fig. 10.20a, is divided into zone 1, that is the zone vertically above the sloping bed, and zone 2, that is the zone vertically above the flat bad (semicircular rim) of the scour hole adjacent to the pier. The upstream edge of the scour hole can be approximately represented by a circular arc up to the azimuthal angle $\theta = \pm 75°$. The width δ_s of zone 2 is expressed as $\varepsilon_w(R - 0.5b)$, where ε_w is a factor (≈ 0.1), R is the radius of the scour hole, that is, $[d_s \cot\phi_d/(1 - \varepsilon_w)] + 0.5b$, and d_s is the scour depth. In cylindrical polar coordinates, the velocity components (u_r, u_θ, u_z) are in r, θ, and z-direction, respectively.

The tangential velocity u_θ is represented by a power law preserving the no-slip condition at the bed

$$\frac{u_\theta}{U} = k_1 \sin\theta G^m \left(J + \frac{z}{d_s} \right)^{1/n} \tag{10.61}$$

Fig. 10.21 Velocity vectors
at the upstream axis of
symmetry of a pier in an
equilibrium scour hole (Dey
and Raikar 2007a)

where

$$
\left.\begin{array}{l}
G(r) = 1 \\[2mm]
J(r) = \dfrac{R - r}{(R - 0.5b)(1 - \varepsilon_{\mathrm{w}})}
\end{array}\right\} \quad \text{for zone 1, that is } 0.5b + \varepsilon_{\mathrm{w}}(R - 0.5b) \leq r \leq R
$$

$$
\left.\begin{array}{l}
G(r) = \dfrac{R - r}{(R - 0.5b)(1 - \varepsilon_{\mathrm{w}})} \\[2mm]
J(r) = 1
\end{array}\right\} \quad \text{for zone 2, that is } 0.5b < r \leq 0.5b + \varepsilon_{\mathrm{w}}(R - 0.5b)
$$

where $k_1 = k_1(U, h, b, d_{\mathrm{s}})$, U is the depth-averaged approaching flow velocity, h is the approaching flow depth, and m and n are the exponents. The values of m and n were obtained as 2.1 and 3.9, respectively.

The radial velocity u_r changes direction in the scour hole. The u_r-distribution along z varies linearly in the scour hole ($z \leq 0$) and follows a power law above it ($z > 0$). On the other hand, the u_r-distribution along r is parabolic. Thus, the expression for u_r is

$$
\frac{u_r}{U} = -k_2 \cos\theta (J + \zeta_1)\left(2\frac{r}{b} - 1\right) \tag{10.62}
$$

where

$$
\zeta_1(z) = 2\frac{z}{d_{\mathrm{s}}} \quad \text{for zone 1, that is } -\frac{(R - r)d_{\mathrm{s}}}{(R - 0.5b)(1 - \varepsilon_{\mathrm{w}})} \leq z \leq 0
$$

$$
\zeta_1(z) = k_3\left(\frac{z}{h}\right)^{1/\alpha} \quad \text{for zone 2, that is } 0 \leq z \leq h
$$

where k_2 and k_3 are the coefficients similar to k_1, $\alpha = \kappa U/u_*$, κ is the von Kármán constant, and u_* is the shear velocity. Note that Eqs. (10.61) and (10.62) violate the no-slip condition at the pier wall and the bed, respectively, and cannot be applicable to the immediate vicinity of them.

The expression for vertical velocity u_z, obtained by integrating the continuity equation (Eq. 2.164), is

$$
\frac{u_z}{U} = -k_1 \cos\theta \frac{d_s}{r} \cdot \frac{n}{1+n} G^m \left(J + \frac{z}{d_s} \right)^{(1+n)/n} + k_2 \cos\theta \frac{z}{r} \left\{ \left(4\frac{r}{b} - 1 \right)(G + \zeta_2) \right.
$$
$$
\left. - \mathrm{sgn}(r) \frac{r}{(R - 0.5b)(1 - \varepsilon_w)} \left(2\frac{r}{b} - 1 \right) \right\}
$$

$$(10.63)$$

where

$$
\zeta_2(z) = \frac{z}{d_s} \quad \text{for zone 1, that is } -\frac{(R-r)d_s}{(R - 0.5b)(1 - \varepsilon_w)} \leq z \leq 0
$$
$$
\zeta_2(z) = k_3 \frac{\alpha}{1+\alpha} \left(\frac{z}{h} \right)^{1/\alpha} \quad \text{for zone 2, that is } 0 \leq z \leq h
$$
$$
\mathrm{sgn}(r) = 1 \quad \text{for zone 1, that is } 0.5b + \varepsilon_w(R - 0.5b) \leq r \leq R
$$
$$
\mathrm{sgn}(r) = 0 \quad \text{for zone 2, that is } 0.5b < r \leq 0.5b + \varepsilon_w(R - 0.5b)
$$

Equation (10.63) produces a strong downflow along the upstream face of the pier and a flow reversal in the scour hole. It however violates the no-slip condition at the pier wall and the bed. Dey et al. gave the expressions for the coefficients as

$$
k_1 = 1.9 Fr^{0.83} \left(\frac{h}{b} \right)^{0.69} \left(\frac{b}{d_s} \right)^2 \quad \wedge \quad Fr = \frac{U}{(gh)^{0.5}}
$$
$$
k_2 = 2 Fr^{0.92} \left(\frac{h}{b} \right)^{0.57} \left(\frac{b}{d_s} \right)^2
$$
$$
k_3 = \frac{0.8}{k_2} \cdot \frac{1+\alpha}{\alpha} \left(2\frac{R}{b} - 1 \right)^{-1}
$$

Dey and Bose (1994) used the expressions for u_r, u_θ, and u_z to compute the bed shear stress in the scour hole by applying the turbulent boundary-layer approach.

10.5.2 Scour Depth Prediction

Scour at piers is influenced by various parameters (Breusers et al. 1977), which are grouped as follows:

1. *Parameters related to the pier*: Size, shape, spacing, number, and orientation with respect to the approaching flow direction.
2. *Parameters related to the bed sediment*: Median particle size, particle size distribution, angle of repose, and cohesiveness.
3. *Parameters related to the approaching flow condition*: Approaching flow velocity, approaching flow depth, shear velocity, and roughness.
4. *Parameters related to the fluid*: Mass density, viscosity, gravitational acceleration, and temperature. Note that the temperature may not be important in scour problems, unless free surface is frozen.
5. *Parameters related to the time*: Time of scour for an evolving scour case.

A large number of empirical equations were proposed by various investigators to estimate the maximum scour depth at piers based on the data from the laboratory experiments and the field measurements. In general, these equations were derived from a limited range of data and are applicable to the conditions similar to those for which they are valid. Though the number of proposed equations for the estimation of maximum scour depth is overwhelming (Dey 1997a; Melville and Coleman 2000), it is however difficult to confirm their adequacy for the design purposes due to limited field measurements. Nevertheless, the design equations proposed by Melville and Coleman (2000), HEC18 (Richardson and Davis 2001), and Sheppard et al. (2014) seem to provide satisfactory estimations.

Melville and Coleman (2000) recommended a design equation for the estimation of maximum scour depth at piers based on empirical factors, called *K*-factors, which account for the effects of pier, flow, and sediment characteristics. The *K*-factors were determined by fitting the curves that overlap the data plots. Thus, the proposed *K*-factors potentially remain adequate from the viewpoint of a safe pier foundation design. The maximum scour depth d_s at a bridge pier formulated as a product of various *K*-factors is given as

$$d_s = K_h K_I K_d K_s K_\alpha K_t \tag{10.64}$$

where K_h is the flow depth–pier size factor, K_I is the flow intensity factor, K_d is the sediment size factor, K_s is the pier shape factor, K_α is the pier alignment factor, and K_t is the time factor. The relationships for the *K*-factors are as follows:

The *flow depth–pier size factor* K_h is the scour depth d_s at a pier of width b for a given value of flow depth h. It is given by

$$\left. \begin{array}{r} K_h(b/h < 0.7) = 2.4b \\ K_h(0.7 \leq b/h < 5) = 2(hb)^{0.5} \\ K_h(b/h \geq 5) = 4.5h \end{array} \right\} \tag{10.65}$$

The *flow intensity factor* K_I is the ratio of the scour depth d_s for a given flow velocity U to that for the threshold flow velocity U_{cr} for the bed sediment motion. Thus, the flow intensity factor K_I represents the effects of flow intensity on scour

depth. It also accounts for the nonuniformity of sediment in terms of average approaching velocity U_a at armor peak. It is given by

$$
\left.
\begin{aligned}
K_{\mathrm{I}} &= \frac{U - (U_a - U_{\mathrm{cr}})}{U_{\mathrm{cr}}}, \quad \text{for} \quad \frac{U - (U_a - U_{\mathrm{cr}})}{U_{\mathrm{cr}}} < 1 \\
K_{\mathrm{I}} &= 1, \quad \text{for} \quad \frac{U - (U_a - U_{\mathrm{cr}})}{U_{\mathrm{cr}}} \geq 1
\end{aligned}
\right\}
\tag{10.66}
$$

where $U_a = 0.8 U_{\mathrm{cra}}$ and U_{cra} is the maximum average velocity for the bed to armor. Note that for uniform sediment, $U_a(\sigma_g < 1.3) = U_{\mathrm{cr}}$. Under varied stream flow velocities over a bed of nonuniform sediment, a process of armoring prevails resulting in an exposure of coarser particles due to washing out of the finer fraction. The armoring effect is to reduce the scour depth. The U_{cr} and U_{cra} can be obtained from

$$
\frac{U_{\mathrm{cr}}}{u_{*\mathrm{c}}} = 5.75 \log\left(5.53\frac{h}{d_{50}}\right), \; \frac{U_{\mathrm{cra}}}{u_{*\mathrm{ca}}} = 5.75 \log\left(5.53\frac{h}{d_{50\mathrm{a}}}\right)
\tag{10.67}
$$

where $u_{*\mathrm{ca}}$ is the threshold shear velocity for median size $d_{50\mathrm{a}}$ of armor particles, $d_{50\mathrm{a}} = d_{\max}/1.8$ and $d_{\max}$ is the maximum bed sediment size. Melville and Coleman suggested that the $u_{*\mathrm{c}}$ can be empirically calculated as $u_{*\mathrm{c}}(0.1\,\mathrm{mm} \leq d_{50} < 1\,\mathrm{mm}) = 0.0115 + 0.0125 d_{50}^{1.4}$ and $u_{*\mathrm{c}}(1\,\mathrm{mm} \leq d_{50} < 100\,\mathrm{mm}) = 0.0305 d_{50}^{0.5} - 6.5 \times 10^{-3} d_{50}^{-1}$.

Here, $u_{*\mathrm{c}}$ is in m s^{-1} and d_{50} in mm. For $u_{*\mathrm{ca}}$, same expressions can be used replacing $u_{*\mathrm{c}}$ by $u_{*\mathrm{ca}}$ and d_{50} by $d_{50\mathrm{a}}$.
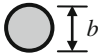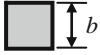
The *sediment size factor* K_d is the ratio of the scour depth d_s for a given value of b/d_{50} to that for b/d_{50} for which d_s becomes maximum and beyond which, there is no effect of b/d_{50} on d_s. For nonuniform sediment, d_{50} is to be replaced by $d_{50\mathrm{a}}$. It is

$$
\left.
\begin{aligned}
K_\mathrm{d}(b/d_{50} \leq 25) &= 0.57 \log\left(2.24\frac{b}{d_{50}}\right) \\
K_\mathrm{d}(b/d_{50} > 25) &= 1
\end{aligned}
\right\}
\tag{10.68}
$$

However, for the piers embedded in gravel-beds, Raikar and Dey (2005b) proposed an additional set of sediment size factor. It is

$$
\left.
\begin{aligned}
K_\mathrm{d}(b/d_{50} \leq 9) &= 0.6 \log\left(3.88\frac{b}{d_{50}}\right) \\
K_\mathrm{d}(9 < b/d_{50} \leq 25) &= 0.184 \log\left(14070\frac{b}{d_{50}}\right) \\
K_\mathrm{d}(b/d_{50} > 25) &= 1
\end{aligned}
\right\}
\tag{10.69}
$$

Table 10.2 Shape factors K_s for pier scour

Shape	Name	K_s
	Circular	1
	Round nosed	1
	Square nosed	1.1
	Sharp nosed	0.9

Fig. 10.22 Oblique alignment of a rectangular pier with respect to approaching flow direction
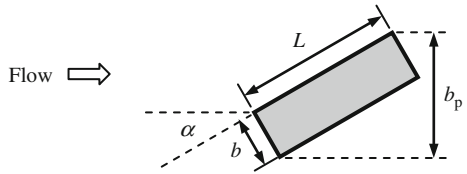
The *shape factor* K_s is defined as the ratio of the scour depth d_s for a particular pier shape to that for the circular pier having a diameter same as the pier width. The shape factors K_s for different piers are furnished in Table 10.2.

The *alignment factor* K_α is the ratio of the scour depth d_s at an oblique pier to that at an aligned pier. In case of noncircular piers, the scour depth increases with an increase in the effective projected width of the piers. The K_α is given by

$$K_\alpha = \left(\frac{b_p}{b}\right)^{0.65} \tag{10.70}$$

where b_p is the projected width of a rectangular pier normal to the approaching flow (= $L\sin\alpha + b\cos\alpha$), α is the pier orientation with respect to the approaching flow or skewness, and L is the pier length (Fig. 10.22). For circular piers, $K_\alpha = 1$.

The *time factor* K_t is the ratio of the scour depth d_s for a given time t to the equilibrium scour depth. It depends on the scour condition, such as clear-water scour and live-bed scour. For live-bed scour, K_t can be approximated as unity, as equilibrium is attained rather rapidly, while for clear-water scour, K_t is given by

$$K_t = \exp\left[-0.03\left|\frac{U_{cr}}{U}\ln\left(\frac{t}{t_e}\right)\right|^{1.6}\right] \tag{10.71}$$

where t_e is the time to reach equilibrium scour depth. It can be calculated from

Table 10.3 Bed condition factors K_{bed} for pier scour

Bed condition	Dune height, η_d (m)	K_{bed}
Clear-water	–	1.1
Plane bed and antidunes	–	1.1
Small dunes	$0.6 \leq \eta_d < 3$	1.1
Medium dunes	$3 \leq \eta_d < 9$	1.1–1.2
Large dunes	$\eta_d \geq 9$	1.3

Table 10.4 Alignment factors K_α for pier scour

α (degree)	$L/b = 4$	$L/b = 8$	$L/b = 12$
0	1	1	1
15	1.5	2	2.5
30	2	2.75	3.5
45	2.3	3.3	4.3
90	2.5	3.9	5

$$\left.\begin{array}{l} t_e(\text{days}) = 48.26\dfrac{b}{U}\left(\dfrac{U}{U_{\text{cr}}} - 0.4\right), \quad \text{for } \dfrac{h}{b} > 6 \text{ and } \dfrac{U}{U_{\text{cr}}} > 0.4 \\[3mm] t_e(\text{days}) = 30.89\dfrac{b}{U}\left(\dfrac{U}{U_{\text{cr}}} - 0.4\right)\left(\dfrac{h}{b}\right)^{0.25}, \quad \text{for } \dfrac{h}{b} \leq 6 \text{ and } \dfrac{U}{U_{\text{cr}}} > 0.4 \end{array}\right\}$$

$$\tag{10.72}$$

At threshold condition ($U = U_{\text{cr}}$), t_e being maximum, when $h > 6b$, is given as

$$t_e(\text{days}) = 28.96\frac{b}{U} \tag{10.73}$$

where b is in m and U in m s^{-1}.

According to HEC18 (Richardson and Davis 2001), the scour depth at a pier in both clear-water and live-bed scour conditions is given by

$$\frac{d_s}{b} = 2K_sK_\alpha K_{\text{bed}}K_a\left(\frac{h}{b}\right)^{0.35}Fr^{0.43} \tag{10.74}$$

where K_{bed} is the factor for bed condition (Table 10.3) and K_a is the factor for armoring of bed sediment. Further, for a maximum value of d_s at a round-nosed pier with aligned flow, if $Fr \leq 0.8$, then $d_s/b \leq 2.4$ and if $Fr > 0.8$, then $d_s/b \leq 3$ (Table 10.4).

The K_a that takes into account of armoring of bed sediment can be given as

$$K_a = 1, \quad \text{for } d_{50} < 2 \text{ mm or } d_{95} < 20 \text{ mm} \tag{10.75a}$$

$$K_a = 0.4U_r^{0.15}, \quad \text{for } d_{50} \geq 2 \text{ mm and } d_{95} \geq 20 \text{ mm} \quad \wedge \quad U_r = \frac{U - U_{crs}|_{d_{50}}}{U_{cr}|_{d_{50}} - U_{crs}|_{d_{95}}}$$

$$(10.75b)$$

where $U_{crs}|_{d_i}$ is the approaching flow velocity required for threshold of scour at a pier with sediment size d_i, $U_{cr}|_{d_i}$ is the threshold flow velocity for bed sediment of size d_i, and d_i is the i-percent finer sediment size. Note that in Eq. (10.75b), U_r should be positive ($U_r > 0$). The $U_{crs}|_{d_i}$ is estimated as

$$U_{crs}|_{d_i} = 0.645 \left(\frac{d_i}{b}\right)^{0.053} U_{cr}|_{d_i} \quad \wedge \quad U_{cr}|_{d_i} = 6.19 h^{1/6} d_i^{1/3} \qquad (10.76)$$

Further, Sheppard et al. (2014) proposed a method of scour depth prediction as

$$\frac{d_s}{b_e} = 2.5 f_1 f_2 f_3, \quad \text{for } 0.4 U_{cr} \leq U < U_{cr} \qquad (10.77a)$$

$$\frac{d_s}{b_e} = f_1 \left[2.2 \left(\frac{U - U_{cr}}{U_{peak} - U_{cr}} \right) + 2.5 f_3 \left(\frac{U_{peak} - U}{U_{peak} - U_{cr}} \right) \right], \quad \text{for } U_{cr} \leq U \leq U_{peak}$$

$$(10.77b)$$

$$\frac{d_s}{b_e} = 2.2 f_1, \quad \text{for } U > U_{peak} \qquad (10.77c)$$

where b_e is the effective pier diameter and U_{peak} is the live-bed peak flow velocity,

$$f_1 = \tanh \left[\left(\frac{h}{b_e} \right)^{0.4} \right], \quad f_2 = 1 - 1.2 \left[\ln \left(\frac{U}{U_{cr}} \right) \right]^2, \quad f_3 = \frac{\dfrac{b_e}{d_{50}}}{0.4 \left(\dfrac{b_e}{d_{50}} \right)^{1.2} + 10.6 \left(\dfrac{b_e}{d_{50}} \right)^{-0.13}},$$

$$\left. \begin{array}{l} U_{peak} = 5 U_{cr}, \text{ if } 5 U_{cr} \geq 0.6 (gh)^{0.5} \\ U_{peak} = 0.6 (gh)^{0.5}, \text{ if } 5 U_{cr} < 0.6 (gh)^{0.5} \end{array} \right\}, \quad b_e = K_s b_p, \quad K_s = 0.86 + 0.97 \left| \alpha - \frac{\pi}{4} \right|^4$$

In the above, α is in radians and $K_s = 1$ for circular piers.

They suggested the empirical relationship for the computation of U_{cr} as

$$U_{cr}(5 \leq \Re \leq 70) = 2.5 u_{*c} \ln \left\{ \frac{73.5 h}{d_{50}} \left[\Re (2.85 + 0.002 \Re - 0.58 \ln \Re) + \frac{111}{\Re} - 6 \right]^{-1} \right\}$$

$$(10.78a)$$

Table 10.5 Equations of equilibrium scour depth at piers proposed by different investigators

References	Formula	Regime	Note
Laursen and Toch (1956)	$\dfrac{d_s}{b} = 1.35\left(\dfrac{h}{b}\right)^{0.3}$	Clear-water	Laursen and Toch's design curves were expressed by Neill (1964)
Shen et al. (1969)	$d_s = 2.23 \times 10^{-4}\left(\dfrac{Ub}{\upsilon}\right)^{0.619}$	Clear-water	
Hancu (1971)	$\dfrac{d_s}{b} = 2.42\left(2\dfrac{U}{U_{cr}} - 1\right)$ $\times \left(\dfrac{U_{cr}^2}{gb}\right)^{1/3}$	Clear-water/ live bed	For live bed, $2\dfrac{U}{U_{cr}} - 1 = 1$
Breusers et al. (1977)	$\dfrac{d_s}{b} = 2\tanh\left(\dfrac{h}{b}\right)K_I K_s K_\alpha$	Clear-water/ live bed	$K_I = 0$, for $\dfrac{U}{U_{cr}} \leq 0.5$ $K_I = 2\dfrac{U}{U_{cr}} - 1$, for $0.5 < \dfrac{U}{U_{cr}} < 1$ $K_I = 1$, for $\dfrac{U}{U_{cr}} \geq 1$
Jain and Fischer (1980)	$\dfrac{d_s}{b} = 1.86\left(\dfrac{h}{b}\right)^{0.5}$ $\times (Fr - Fr_c)^{0.25}$	Live bed	$Fr_c = \dfrac{U_{cr}}{(gh)^{0.5}}$
Jain (1981)	$\dfrac{d_s}{b} = 1.84\left(\dfrac{h}{b}\right)^{0.3} Fr_c^{0.25}$	Sediment threshold	
Dey (1999)	$\dfrac{d_s}{b} = 1.77\left(\dfrac{h}{b}\right)^{0.15}$	Sediment threshold	

$$U_{cr}(\Re > 70) = 2.5 u_{*c}\ln\left(2.21\,\frac{h}{d_{50}}\right) \tag{10.78b}$$

where

$$\Re = \frac{u_{*c} d_{50}}{2.32 \times 10^{-7}},\text{ and}$$

$$u_{*c} = \left\{16.2 d_{50}\left[\frac{9.09 \times 10^{-6}}{d_{50}} - d_{50}(38.76 + 9.6\ln d_{50}) - 0.005\right]\right\}^{0.5}$$

Besides the aforementioned scour predictors that can produce potentially safe results for the scour depth, Table 10.5 furnishes some empirical equations of equilibrium scour depth proposed by different investigators.

Regarding the maximum limit of scour depth at circular piers, Melville and Coleman (2000) [also Melville and Sutherland (1988)] reported $d_s \leq 2.4b$ for flow Froude number $Fr < 1$. On the other hand, $d_s \leq 3b$ was recommended by HEC18 (Richardson and Davis 2001) and Jain and Fischer (1979). In the experiments conducted by Jain and Fischer (1979), the Fr was as high as 1.5 for the bed conditions of antidunes. However, for noncircular piers, these maximum limits increase and are to be corrected for pier shape and skewness, if any.

Fig. 10.23 Photograph of a wing-wall abutment. Photograph by the author

Fig. 10.24 Photograph of an equilibrium scour hole at a wing-wall abutment in a flume

10.6 Scour at Bridge Abutments

Abutments, located at either end of a bridge span, are the substructures over which the bridge superstructure rests (Fig. 10.23). Akin to bridge piers, they also help to transmit the weight of the bridge including traffic to the foundation bed. Piers are located within the bridge span (Sect. 10.5). Scour at bridge abutments is also equally or even more responsible for failure of bridges as compared to scour at piers. Similar to bridge piers, the flow separates at the upstream of the abutment as it travels by the side of the abutment, creating a vortex trail to move downstream. The result is that the sediment bed in the vicinity of the abutment is scoured, exposing the abutment foundation that may lead to the failure of the bridge.

A study of the US Federal Highway Administration in 1973 concluded that of 383 bridge failures, 25 % involved pier damage and 72 % involved abutment damage (Richardson et al. 1993). In a report submitted to the National Roads Board of New Zealand, Sutherland (1986) pointed out that of the 108 bridge failure records, 29 were attributed to abutment scour during 1960–1984. According to Kandasamy and Melville (1998), 6 out of 10 bridge failures that occurred in New Zealand during Cyclone Bola were related to the abutment scour. In another report of the Department of Scientific and Industrial Research of New Zealand, Macky (1990) mentioned that about 50 % of total expenditure was made toward the bridge damage repairing and maintenance, out of which 70 % was spent toward the abutment scour. Therefore, abutment scour, due to its practical importance, was studied extensively by various researchers [see the review by Barbhuiya and Dey (2004)]. Figure 10.24 shows the photograph of an equilibrium scour hole at a wing-wall abutment in an experimental flume. It gives an idea about the shape of the scour hole that occurs at an abutment.

The flow field at an abutment is complex in detail, and the complexity increases with the development of scour hole involving flow separation to develop three-dimensional vortex flow. Kwan and Melville (1994) [also in Kwan (1988)] used a hydrogen bubble technique to measure the three-dimensional flow field in a scour hole at a wing-wall abutment. They identified a *primary vortex*, which is quite similar to the horseshoe vortex at a pier, along with the *downflow* being the principal mechanism of scour at an abutment. On the upstream face of an abutment, a vertical pressure gradient is developed due to the stagnation of approaching flow by the abutment. The pressure gradient drives the fluid downward to roll up. Thus, primary vortex is developed and it enlarges its size with the development of the scour hole. They also reported that the primary vortex and the downflow are confined mainly in the scour hole beneath the line of the original bed level. The primary vortex is elliptical in shape with an inner core region as that of a forced vortex and an outer core region as that of a free vortex. The maximum velocity and downflow component in the vicinity of the abutment were measured as 1.35 and 0.75 times the approaching flow velocity, respectively. They also
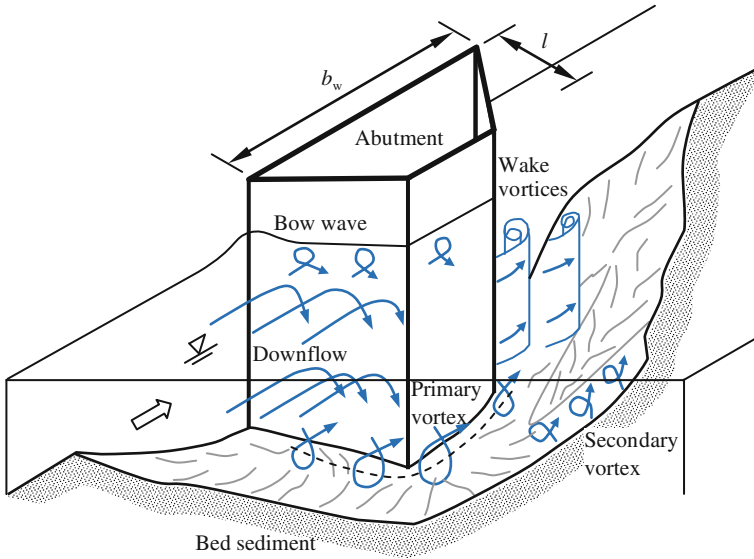
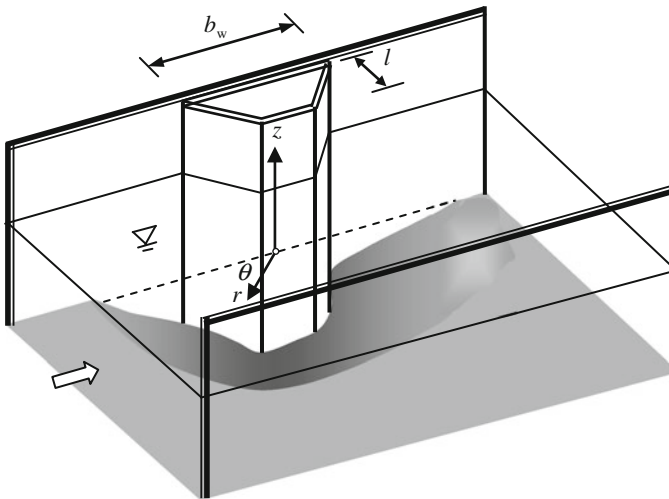**Fig. 10.25** Schematic of flow field at an abutment (Kwan 1988)

Fig. 10.26 Coordinate system for representation of flow and schematic of a scour hole at a 45° wing-wall abutment

identified a *secondary vortex* with counter rotational direction to that of the primary vortex occurring next to the primary vortex. The secondary vortex is believed to have the effect of restricting the scouring capacity of the primary vortex. In the downstream of abutment, *wake vortices* are created due to the
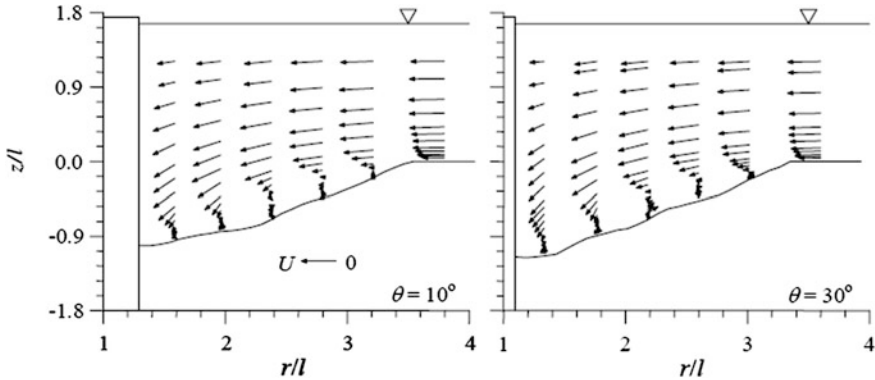
Fig. 10.27 Normalized velocity vectors at azimuthal sections ($\theta = 10^\circ$ and 30°) of a 45° wing-wall abutment after Dey and Barbhuiya (2006)

separation of flow at the upstream and downstream of the abutment corners. The unstable shear layers created due to the flow separation roll up to form eddy structures, termed *wake vortices*. The wake vortices drifted downstream by the mean flow act like small tornadoes lifting up sediment particles from the bed. The wake vortices are rather weak as compared to the primary vortex. Bow wave having a rotational motion opposite to that of primary vortex appears on the upstream face of the abutment near the free surface. The major flow components at a wing-wall abutment identified by Kwan (1988) are shown schematically in Fig. 10.25.

Dey and Barbhuiya (2005a, b, 2006) investigated the three-dimensional tur-bulent flow fields at semicircular, vertical-wall and 45° wing-wall abutments, embedded in a stabilized equilibrium scoured bed by using an ADV [also in Barbhuiya (2003)]. A cylindrical polar coordinate system, as shown in Fig. 10.26, was used by Dey and Barbhuiya (2006) to represent the normalized velocity vectors at azimuthal sections of a 45° wing-wall abutment with a scour hole. Figure 10.27 shows velocity vectors at $\theta = 10^\circ$ and 30° (Dey and Barbhuiya 2006). Here, z is the vertical distance, r is the radial distance, and l is the abutment length transverse to the flow. The characteristics of vortex flow inside the scour hole (that is, in the flow zone $z \leq 0$) together with the strong downflow along the upstream face of the abutment are evident. Note that as the length scales of the axes (ordinate and abscissa) are different in Fig. 10.27, the vortices are apparently stretched horizontally, but they are actually not so. The circulation is strong at the upstream of the abutment and decreases with an increase in θ. Above the scour hole (that is, in the flow zone $z > 0$), the flow is horizontal for $r > 3l$, and then, it gradually curves down toward the abutment.

10.6.1 Scour Depth Prediction

Parameters involved in scour phenomenon at abutments can be grouped in the similar way as those of pier scour (Sect. 10.5.2), except the following two parameters:

1. *Parameters related to the abutment*: Size, shape, and orientation with respect to the approaching flow direction.
2. *Parameters related to the geometry of channel*: Width, cross-sectional shape, and slope.

Most of the scour predictors were preliminarily obtained, as functional relationships, using the dimensional analysis based on the aforementioned parameters. Then, experimental and field data were used to give them a final shape as empirical equations. Proposed empirical equations for the estimation of maximum scour depth at abutments are overwhelming (Barbhuiya and Dey 2004), but their application is limited to the conditions similar to those for which they were validated. The design approaches proposed by Melville and Coleman (2000) and Froehlich (1989), which was recommended by HEC18 (Richardson and Davis 2001), for the estimation of maximum scour depth at abutments based on K-factors seem to be adequate from the viewpoint of the safety of abutment foundation.

According to Melville and Coleman (2000), the maximum equilibrium scour depth d_s at an abutment for both clear-water and live-bed conditions is given by

$$d_s = K_h K_I K_d K_s K_\alpha K_G K_t \qquad (10.79)$$

where K_G is the channel geometry factor and other K-factors are designated similar to that in Eq. (10.64). The relationships for K-factors, in case of abutment scour, are given as follows:

The *flow depth–pier size factor K_h* for abutment scour is

$$\left.\begin{array}{c} K_h(l/h \leq 1) = 2l \\ K_h(1 < l/h < 25) = 2(hl)^{0.5} \\ K_h(l/h \geq 25) = 10h \end{array}\right\} \qquad (10.80)$$

The above K_h-factor is based on Melville (1992) who distinguished short and long abutments. For short abutments ($l/h \leq 1$), the scour depth d_s is independent of flow depth h and dependent on abutment length l. For long abutments ($l/h \geq 25$), the d_s is dependent on h and independent of l. For $1 < l/h < 25$, the d_s is dependent on both l and h. Note that l is projected length for skewed abutments (Fig. 10.28).

The *flow intensity factor K_I* given by Eq. (10.66) for the case of pier scour is also applicable for the abutment scour.

Fig. 10.28 Oblique
alignment of an abutment
(*plan view*)
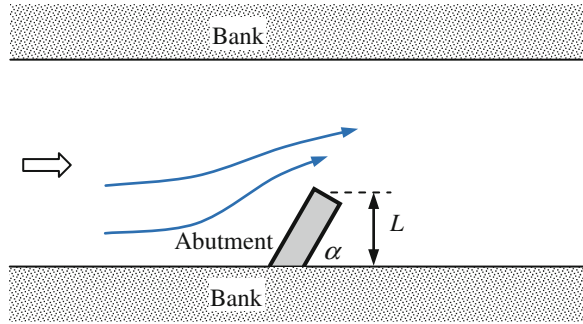
The *sediment size factor* K_d for abutment scour is

$$\left.\begin{array}{l} K_d(l/d_{50} \leq 25) = 0.57\log\left(2.24\dfrac{l}{d_{50}}\right) \\ K_d(l/d_{50} > 25) = 1 \end{array}\right\} \tag{10.81}$$

However, for the abutments embedded in gravel-beds, Raikar and Dey (2005a) proposed new sediment size factors as

$$\left.\begin{array}{l} K_d(l/d_{50} \leq 10) = 1.184\log\left(0.588\dfrac{l}{d_{50}}\right) \\ K_d(10 < l/d_{50} \leq 25) = 0.226\log\left(1052.8\dfrac{l}{d_{50}}\right) \\ K_d(l/d_{50} > 25) = 1 \end{array}\right\} \tag{10.82}$$

The *shape factor* K_s is defined as the ratio of the scour depth d_s for a given abutment shape to that for the vertical-wall abutment having a same length. The shape factors K_s for different abutments are given in Table 10.6.
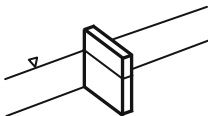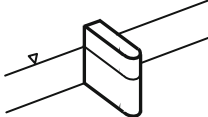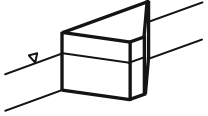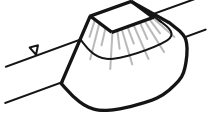
For abutments, the values of *alignment factor* K_α for abutment scour are

$$\left.\begin{array}{l} K_\alpha(l/h \geq 3) = K_\alpha^* \\ K_\alpha(1 < l/h < 3) = K_\alpha^* + (1 - K_\alpha^*)\left(1.5 - 0.5\dfrac{b}{h}\right) \\ K_\alpha(l/h \leq 1) = 1 \end{array}\right\} \tag{10.83}$$

The values of K_α^* in the above equation are obtained from Table 10.7.

The *channel geometry factor* K_G is defined as the ratio of the scour depth d_s at an abutment to that at the same abutment in the equivalent rectangular channel. In case of rectangular channels, $K_G = 1$. However, for abutments in compound channels, K_G depends on the abutment position in the compound channel. The K_G is

Table 10.6 Shape factors K_s for abutment scour

Shape	Name	K_s
	Vertical-wall	1
	Semicircular ended	0.75
	45° wing-wall	0.75
	Spill-through (Horizontal:Vertical)	
	0.5:1	0.6
	1:1	0.5
	1.5:1	0.45

Table 10.7 Factors K_α^* for abutment scour

α (degree)	30	45	60	90	120	135	150
K_α^*	0.9	0.95	0.98	1	1.05	1.07	1.08

$$K_G = \left\{ 1 - \left(\frac{l^*}{l}\right)\left[1 - \left(\frac{h^*}{h}\right)^{5/3}\left(\frac{n}{n^*}\right)\right]\right\}^{0.5} \tag{10.84}$$

where l^* is the abutment length spanning the flood channel, h^* is the flow depth in the flood channel, and n and n^* are the Manning roughness coefficients in the main and flood channels, respectively. In case of an inclined abutment, l and l^* are the projected abutment length and that spanning the flood channel, respectively.

For live-bed scour, the *time factor* K_t is unity; while for clear-water scour, K_t for abutment scour is given by

$$K_t = 0.1 \frac{U_{cr}}{U} \ln\left(\frac{t}{t_e}\right) + 1 \tag{10.85}$$

Table 10.8 Shape factors K_s for abutment scour

Abutment shape	K_s
Vertical-wall	1
Vertical-wall abutment with wing walls	0.82
Spill-through	0.55

The time t_e to reach equilibrium scour depth is given by

$$\left.\begin{array}{l} t_e(\text{days})(l/h \geq 1.2) = 25\dfrac{h}{U} \\[2mm] t_e(\text{days})(l/h < 1.2) = 20.83\dfrac{h}{U} \end{array}\right\} \qquad (10.86)$$

HEC18 (Richardson and Davis 2001) recommended Froehlich's (1989) equation of live-bed scour at abutments. The estimation of maximum scour depth is

$$\frac{d_s}{l} = 2.27 K_s K_\alpha \left(\frac{h}{l}\right)^{0.57} Fr^{0.61} + 1 \qquad (10.87)$$

where $Fr = U_0/(gh)^{0.5}$, $U_0 = Q_0/A_0$, Q_0 is the flow rate obstructed by the abutment and approach embankment, and A_0 is the flow area of the approach cross section obstructed by the embankment. The values of *shape factors* K_s are furnished in Table 10.8.

The *alignment factor* K_α is given by

$$K_\alpha = \left(\frac{\alpha}{90}\right)^{0.13} \qquad (10.88)$$

where α is the downstream angle of inclination of abutment with bank (Fig. 10.28), such that $\alpha < 90°$ is for the abutment pointing downstream and $\alpha > 90°$ for pointing upstream.

Table 10.9 furnishes some additional empirical scour depth predictors at abutments proposed by various investigators.

10.7 Scour Countermeasures

Engineering devices for countermeasure of scour at bridge piers are generally classified into two categories: *Flow-altering* and *bed-armoring countermeasures*. The working principle of flow-altering countermeasures is to diminish the strength of the downflow and the horseshoe vortex, which are the primary cause of pier scour. Of various types of flow-altering countermeasures, slot in a pier (Grimaldi et al. 2009), spirally wrapped cables on a pier (Dey et al. 2006), collars and horizontal plates attached to a pier (Kim et al. 2005; Parker et al. 1998),

Table 10.9 Equations of equilibrium scour depth at abutments proposed by various investigators

References	Formula	Regime	Note
Laursen (1963)	$\frac{d_s}{l} = 1.89\left(\frac{h}{l}\right)^{0.5}$	Sediment threshold	
Liu et al. (1961)	$\frac{d_s}{l} = 1.1\left(\frac{h}{l}\right)^{0.6} Fr^{0.33}$	Live bed	Spill-through abutments
	$\frac{d_s}{l} = 2.15\left(\frac{h}{l}\right)^{0.6} Fr^{0.33}$	Live bed	Wing- and vertical-wall abutments
	$\frac{d_s}{l} = 12.5\frac{h}{l} \cdot \frac{B_1 Fr}{B_2}$	Clear-water	Vertical-wall abutments
Gill (1970, 1972)	$\frac{d_s}{l} = 8.375\left(\frac{h}{l}\right)^{0.75}\left(\frac{d_{50}}{l}\right)^{0.25}\left(\frac{B}{B-l}\right)^{6/7} - \frac{h}{l}$	Sediment threshold	B is the approach stream width
Sturm and Janjua (1994)	$\frac{d_s}{l} = 7.7\frac{h}{l}\left(\frac{1}{M}\cdot\frac{U}{U_{cr}} - 0.35\right)$	Clear-water and live bed	M is the discharge contraction ratio*
Lim (1997)	$\frac{d_s}{l} = K_s\frac{h}{l}\left\{\frac{0.9F_d^{0.75}}{\Theta_c^{0.375}}\left(\frac{d}{h}\right)^{0.25}\left[0.9\left(\frac{l}{h}\right)^{0.5} +1\right] - 2\right\}$	Clear-water	$F_d = \dfrac{U}{(\Delta g d_{50})^{0.5}}$
Kandasamy and Melville (1998)	$\frac{d_s}{l} = K_s K_h\left(\frac{h}{l}\right)^{m}$	Clear-water and live bed	$K_h = 5$ and $m = 1$ for $h/l \leq 0.04$, $K_h = 1$ and $m = 0.5$ for $0.04 < h/l < 1$, and $K_h = 1$ and $m = 0$ for $h/l > 1$
Dey and Barbhuiya (2004)	$\frac{d_s}{l} = 5.857\left(\frac{U_{cr}}{\Delta g l}\right)^{0.314}\left(\frac{h}{l}\right)^{0.128}\left(\frac{d_{50}}{l}\right)^{0.167}$	Clear-water	Vertical-wall abutments
	$\frac{d_s}{l} = 6.483\left(\frac{U_{cr}}{\Delta g l}\right)^{0.312}\left(\frac{h}{l}\right)^{0.101}\left(\frac{d_{50}}{l}\right)^{0.231}$	Clear-water	45° wing-wall abutments
	$\frac{d_s}{l} = 7.287\left(\frac{U_{cr}}{\Delta g l}\right)^{0.192}\left(\frac{h}{l}\right)^{0.103}\left(\frac{d_{50}}{l}\right)^{0.296}$	Clear-water	Semicircular abutments

*M that is termed *discharge contraction ratio* is defined as the ratio of the discharge at approach section through the opening width to the total discharge

Fig. 10.29 Typical
placement of a riprap layer at
a pier
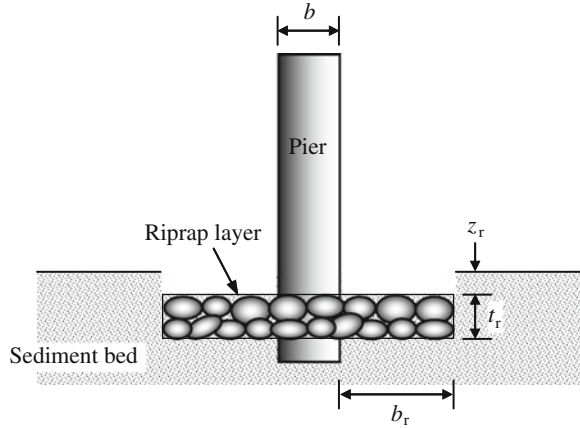
arrangement of sacrificial piles (Melville and Hadfield 1999; Chiew and Lim 2003; Haque et al. 2007), and flow deflection by upstream vanes or plates (Odgaard and Wang 1991; Lauchlan 1999) are pertinent. Tafarojnoruz et al. (2010) compiled a review of literature on flow-altering countermeasures at piers. On the other hand, bed-armoring countermeasures provide a physical barrier against scour. In practice, these barriers often consist of large and heavy units, which cannot be easily removed by the flow at piers (Melville and Coleman 2000; Lagasse et al. 2007; Melville et al. 2008). The most commonly employed protection of bridge piers (and also abutments) is the use of a riprap layer around the piers. In this section, riprap protection at piers is mainly discussed.

Figure 10.29 shows a schematic of the placement of a riprap layer at a pier of width b, considering the flow to be the normal to the plane of the drawing. Parameters involved in riprap protection design at piers are as follows:

1. Thickness t_r of riprap layer.
2. Coverage b_r of riprap layer at sides, upstream, and downstream of a pier.
3. Placement z_r of riprap layer with respect to the original bed level.
4. Median size d_{50r} of riprap stones and their gradation.

The thickness of the riprap layer is recommended typically in the range $t_r = 2$–$3d_{50r}$. Thicker layer can resist higher flow intensity (Chiew 1995). The general recommendation for riprap coverage is to place riprap around a pier extending up to $b_r = 3b$ from the pier wall in all directions (Parola 1995; Croad 1997; Parker et al. 1998; Lauchlan 1999). Parker et al. (1998) suggested b_r for rectangular piers is $b_r = 1.5b/\cos\alpha$. Regarding the placement of a riprap layer z_r, the surface of the riprap layer to be placed at the original streambed level is the common recommendation (Richardson and Davis 2001). Another recommendation is to place the riprap layer below the possible general scour depth level (Neill 1973; Breusers et al. 1977). Further, to improve the performance of a riprap protection, the use of a filter layer beneath the riprap layer is generally proposed. Filters that can be granular filters or synthetic filters prevent the passage of finer

bed sediment through the highly porous riprap layers, but also have sufficient permeability to prevent building up water pressure within the underlying bed sediment. Regarding riprap stones, it is important that they should be well graded, such that the maximum stone size should not exceed twice the median size of riprap stones, that is, $d_{max} \leq 2d_{50r}$ (Richardson and Davis 2001), and the median size should not exceed twice the 15 % finer stone size, that is, $d_{50r} \leq 2d_{15r}$ (Croad 1997). To determine the riprap stone size d_{50r}, HEC-18 (Richardson and Davis 2001) and HEC-23 (Lagasse et al. 2001) recommended using the reorganized form of Isbash (1936) equation. It is

$$d_{50r} = 0.346 \frac{(KU)^2}{\Delta g} \qquad (10.89)$$

where K is the pier shape coefficient. The values of K are that for round-nosed piers, $K = 1.5$ and for rectangular piers, $K = 1.7$.

Further, Lauchlan (1999) suggested an equation of riprap stone size taking into account the placement depth z_r below the original bed level. It is

$$d_{50r} = 0.3f_{SF}h\left(1 - \frac{z_r}{h}\right)^{2.75} Fr^{1.2} \qquad (10.90)$$

where f_{SF} is a safety factor that has a minimum recommended value of 1.1.

In case of riprap protection at abutments, the coverage b_r of riprap layer around an abutment, called *launching apron*, is extended up to $b_r = 1.5d_s$ from the abutment wall in all directions. It should have a minimum thickness of $t_r = 2d_{50r}$. The spill-through abutments are additionally protected by stone-pitching on the slant face of the abutment. The median stone size d_{50r} of the riprap layer can be obtained from the equation given by Austroads (1994) as

$$d_{50r} = 1.026 \frac{hFr^2}{\Delta} \qquad (10.91)$$

According to Atayee et al. (1993) and Richardson and Davis (2001), the median stone size can be obtained as

$$d_{50r}(Fr_2 \leq 0.8) = K_s \frac{h_2 Fr_2^2}{\Delta} \qquad (10.92a)$$

$$d_{50r}(Fr_2 > 0.8) = K_s \frac{h_2 Fr_2^{0.14}}{\Delta} \qquad (10.92b)$$

where h_2 is the flow depth in the contracted section of the bridge, Fr_2 is the flow Froude number in the contracted section [$= U_2/(gh_2)^{0.5}$], and U_2 is the average flow velocity in the contracted section. The values of the shape factor K_s are 0.89 ($Fr \leq 0.8$) and 0.61 ($Fr > 0.8$) for spill-through abutments and 1.02 ($Fr \leq 0.8$) and 0.69 ($Fr > 0.8$) for vertical-wall abutments.

10.8 Appendix

10.8.1 Submerged Wall Jets (Dey et al. 2010)

Submerged plane wall jet is described as a fluid jet that impinges tangentially (or at an angle) on a solid boundary surrounded by the same fluid (still or moving) progressing along the solid boundary (Fig. 10.30a). By virtue of the initially abounding momentum, the streamwise velocity $\bar{u}$ in the shear flow of jet exceeds that in external stream over a downstream reach (Launder and Rodi 1981). In a submerged wall jet, the flow zone of principal importance is the fully developed zone existing after the developing zone of jet (Fig. 10.30b). The jet is confined to a solid boundary on one side, and the other side is fluid bounded. The jet layer is overlain by a circulatory flow having an enormous mixing of fluid with a flow reversal. Since the boundary conditions for a submerged wall jet are such that the velocities at the solid boundary and on the separation line are zero ($\bar{u} = 0$), the velocity distribution has a peak within the jet layer. Below the peak velocity level (in the inner layer), the flow is characterized by a boundary-layer flow, and the upper flow zone is structurally similar to a free jet. Therefore, a submerged wall jet, characterized by a shear flow influenced by the solid boundary and an over-lying circulatory flow layer, is of self-similar type of flow (Dey et al. 2010).

A typical $\bar{u}$-distribution in the fully developed zone describing various layers of flow is shown in Fig. 10.30a. The inner layer and outer layer of jet refer to the zones below and above the point of occurrence of peak velocity u_0, called the *jet velocity*. Precisely, the jet layer ($0 \leq z \leq \delta$) that comprises of inner layer and outer layer extends up to the inflection point (that is, the point of change of sign of slope, $d\bar{u}^2/dz^2 = 0$) of a $\bar{u}$-distribution. Above the jet layer, there exists a circulatory flow layer that is divided by the separation line $\bar{u} = 0$ into inner layer and outer layer of the circulatory flow. The flow in the outer layer of the circulatory flow is directed toward upstream. Momentum exchange takes place through the separation line within the circulatory flow layer of the jet. The jet layer thickness δ is important from the viewpoint of scaling the vertical distance z (Dey et al. 2010).

A two-dimensional submerged plane wall jet issuing from a sluice opening is considered as the jet emerges in the form of a bunch of diverging streamlines. Another bunch of streamlines constitutes a circulatory flow above the jet in the circulatory flow layer. The limiting streamline on the solid boundary has a velocity $\bar{u} = 0$ due to no-slip. Let the equation of the jet layer be $z = \delta(x_1)$, where $x_1 = x + x_0$, extending up to the inflection point of $\bar{u}$-distribution. The jet layer is assumed as a boundary layer. Due to finite size of issuing jet, the point of emergence (that is the origin) of the jet is located upstream of the sluice opening at a certain distance x_0. Applying the boundary-layer approximation to the two-dimensional Reynolds-averaged Navier–Stokes (RANS) equations of steady flow and eliminating pressure term, the following equation is obtained (Rajaratnam 1976):

(a)

(b)
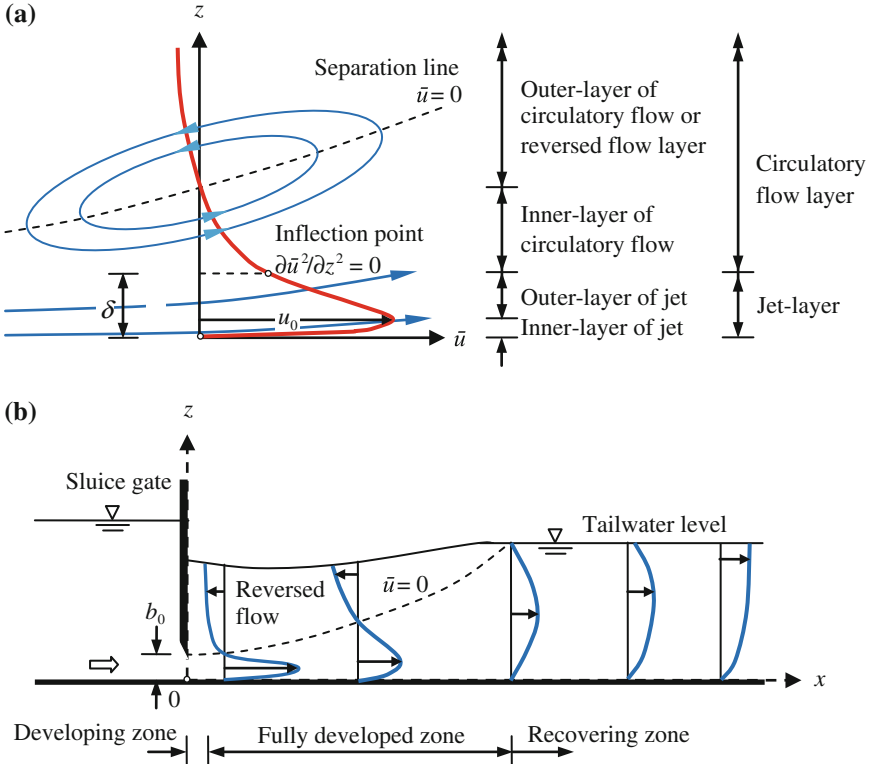
Fig. 10.30 a Typical sketch of $\bar{u}$-distribution superimposed on the flow field in the fully developed flow zone and **b** flow zones in a submerged wall jet (Dey et al. 2010)

$$\bar{u}\frac{\partial \bar{u}}{\partial x} + \bar{w}\frac{\partial \bar{u}}{\partial z} + \frac{\partial \overline{u'w'}}{\partial z} + \frac{\partial}{\partial x}\left(\overline{u'u'} - \overline{w'w'}\right) = v\frac{\partial^2 \bar{u}}{\partial z^2} \qquad (10.93)$$

The continuity equation is

$$\frac{\partial \bar{u}}{\partial x} + \frac{\partial \bar{w}}{\partial z} = 0 \qquad (10.94)$$

The flow in submerged plane wall jets is characterized by the self-similar class. To obtain the similarity solutions of Eqs. (10.93) and (10.94) by the transformation $\eta = z/\delta(x_1)$, where the horizontal length scale x_1 is dimensional for the theory, the solutions are of the form

$$\bar{u} = u_0\,\varphi(\eta), \ \overline{u'w'} = -u_0^2\,\psi(\eta), \ \overline{u'u'} - \overline{w'w'} = u_0^2\,\sigma(\eta) \qquad (10.95)$$

where $u_0 = u_0(x_1)$. It is pertinent to mention that a wall jet boundary layer is not amenable to similarity analysis, unless different scaling laws are assumed for the inner layer and the outer layer of the jet (Barenblatt et al. 2005). Inserting the above expressions into Eq. (10.93) and using Eq. (10.94), one obtains

$$\frac{\delta}{u_0} \cdot \frac{\mathrm{d}u_0}{\mathrm{d}x} \varphi^2 - \left(\frac{\mathrm{d}\delta}{\mathrm{d}x} + \frac{\delta}{u_0} \cdot \frac{\mathrm{d}u_0}{\mathrm{d}x}\right) \varphi' \int\limits_0^\eta \varphi \mathrm{d}\eta - \psi' = \frac{1}{R_\delta} \varphi'' - \frac{2\delta}{u_0} \cdot \frac{\mathrm{d}u_0}{\mathrm{d}x}\sigma + \frac{\mathrm{d}\delta}{\mathrm{d}x}\sigma' \approx 0$$

$$(10.96)$$

where $R_\delta = u_0\delta/v$. The right-hand side of Eq. (10.96) vanishes, as the terms containing the difference of streamwise and vertical Reynolds normal stresses represented by σ are negligible and R_δ is too large. For a similarity solution, Eq. (10.96) must be independent of x or x_1 (Schwarz and Cosart 1961), that is

$$\frac{\mathrm{d}\delta}{\mathrm{d}x_1} = \beta, \quad \frac{\delta}{u_0} \cdot \frac{\mathrm{d}u_0}{\mathrm{d}x_1} = -\beta\alpha \qquad (10.97)$$

where β and α are constants. Hence, by integration, one can write

$$\delta = \beta x_1, \quad u_0 = \beta_0 x_1^{-\alpha} \qquad (10.98)$$

where β_0 is a constant. Noticeably, the δ increases linearly with x_1, and u_0 varies as $x_1^{-\alpha}$. For a free jet, α is 0.5 (Schlichting 1979).

The velocity distribution obtained using Eqs. (10.96) and (10.98) is given by

$$\alpha\varphi^2 + (1-\alpha)\varphi' \int\limits_0^\eta \varphi \mathrm{d}\eta + \frac{1}{\beta}\psi' = 0 \qquad (10.99)$$

Setting $\varphi(\eta) = f'(\eta)$, Eq. (10.99) becomes

$$\alpha f'^2 + (1-\alpha)ff'' + \frac{1}{\beta}\psi' = 0 \qquad (10.100)$$

By definition of the turbulence diffusivity ε_t, one can write

$$\overline{u'w'} = -\varepsilon_t \frac{\partial \bar{u}}{\partial z} = -u_0^2\psi \qquad (10.101)$$

Using Eq. (10.95), Eq. (10.101) yields

$$\psi = \frac{\varepsilon_t}{u_0^2} \cdot \frac{\partial}{\partial z}(u_0\varphi) = \frac{\varepsilon_t}{u_0\delta}\varphi' = \frac{\varepsilon_t}{\beta_0\beta} \cdot \frac{\varphi'}{x_1^{1-\alpha}} = \frac{\bar{\varepsilon}_t}{\beta_0\beta}f'' \qquad (10.102)$$

In Eq. (10.102), the left-hand side being independent of x_1 implies that ε_t is proportional to $x_1^{1-\alpha}$, and hence, $\varepsilon_t = \bar{\varepsilon}_t x_1^{1-\alpha}$. In the narrow turbulent jet layer, $\bar{\varepsilon}_t$ may be assumed to be an averaged value of ε_t over η. Thus, one obtains

$$\alpha f'^2 + (1-\alpha)ff'' + \frac{\bar{\varepsilon}_t}{\beta_0 \beta^2} f''' = 0 \qquad (10.103)$$

The velocity distribution contains an arbitrary constant β_0. Replacing β_0 by $4\bar{\varepsilon}_t/\beta^2$ in Eq. (10.103), one gets the following equation for f:

$$\alpha f'^2 + (1-\alpha)ff'' + \frac{1}{4}f''' = 0 \qquad (10.104)$$

The boundary conditions applicable for the solution of Eq. (10.104) are that at the peak velocity of the jet $f'(\eta = \eta_0) = \varphi(\eta = \eta_0) = 1$, $f(\eta = \eta_0) = 0$ (that is $\bar{w} = 0$), and $f'(\eta \to \infty) = 0$ (that is $\bar{u} = 0$). For a free jet, $\eta_0 = 0$ and $\alpha = 0.5$ (Schlichting 1979), and the solution of Eq. (10.104) is $f = \tanh \eta$. It is anticipated that due to the submergence, α is modified as

$$\alpha = 0.5 + \alpha_1 \qquad (10.105)$$

where α_1 is an additional term mainly due to submergence. The solution of Eq. (10.104) can be given by

$$f(\eta) = \tanh(\eta - \eta_0) + \alpha_1 G(\eta) \qquad (10.106)$$

Substituting Eq. (10.106) into Eq. (10.104) and equating the coefficients of α_1, the differential equation for G is given by

$$G''' + 2\tanh(\eta - \eta_0)G'' + 4\mathrm{sech}^2(\eta - \eta_0)[G' - \tanh(\eta - \eta_0)G \\ + \tanh^2(\eta - \eta_0) + 1] = 0 \qquad (10.107)$$

with boundary conditions $G(\eta = \eta_0) = 0$, $G'(\eta = \eta_0) = 0$, and $G'(\eta \to \infty) = 0$. Equation (10.107) that has highly nonlinear coefficients is a linear differential equation. Galerkin's method is applied to obtain an approximate analytical solution. For this purpose, it is recognized that a function of the pattern of the leading term of Eq. (10.106) that satisfies the boundary condition is

$$G(\eta) = a_0 \tanh^2(\eta - \eta_0) \qquad (10.108)$$

Substituting Eq. (10.108) into Eq. (10.107) and taking the weighted average with the weight appearing in the equation yield

$$a_0 \int_0^\infty \mathrm{sech}^2\eta \ \tanh^3 \eta \ (5 - 9\tanh^2 \eta)\,\mathrm{d}\eta \approx - \int_0^\infty \mathrm{sech}^2\eta \ \tanh^2 \eta \ (1 + \tanh^2 \eta)\,\mathrm{d}\eta$$

(10.109)

Numerically evaluating the integrals in Eq. (10.109), one obtains $a_0 \approx 32/15$. Differentiating Eq. (10.106) with the value of a_0 in Eq. (10.108), one gets

$$\varphi(\eta) = \mathrm{sech}^2(\eta - \eta_0) \left[1 + \frac{64}{15}\alpha_1 \tanh(\eta - \eta_0) \right]$$

(10.110)

Giving the velocity distribution of a submerged wall jet by Eqs. (10.95) and (10.98), the profile holds for $\eta \geq \eta_0$, because below the point of η_0 (that is, within the inner layer of the jet), boundary effects come into account.

In the near-boundary zone (that is, within the inner layer of the jet) $0 \leq \eta \leq \eta_0$, the $1/m$-th power law for $\varphi(\eta)$ can be assumed as in case of a flow over a solid plate. Noting that as $\varphi(\eta = \eta_0) = 1$, $\varphi'(\eta = \eta_0) = 0$, such a law is

$$\varphi(\eta) = \frac{1}{m} \left(\frac{\eta}{\eta_0} \right)^{1/m} \left(1 + m - \frac{\eta}{\eta_0} \right)$$

(10.111)

The Reynolds shear stress τ_{xz} is given by using Eqs. (10.101) and (10.102). It is

$$-\overline{u'w'} = \frac{\beta_0 \bar{\varepsilon}_t}{\beta} x_1^{-2\alpha} \varphi'(\eta)$$

(10.112a)

$$\Rightarrow \tau_{xz} = -\rho \overline{u'w'} = \rho U_0^2 \xi \, (\hat{x} + \hat{x}_0)^{-2\alpha} \varphi'(\eta)$$

(10.112b)

where $\xi = \beta_0 \bar{\varepsilon}_t / (\beta U_0^2 b_0^{2\alpha})$, $\hat{x} = x/b_0$, and $\hat{x}_0 = x_0/b_0$.

From Eqs. (10.110) and (10.111), the following expressions for φ' are obtained:

$$\varphi'(\eta \geq \eta_0) = -\mathrm{sech}^2(\eta - \eta_0) \left\{ 2\tanh(\eta - \eta_0) + \frac{64}{15}\alpha_1 [2\tanh^2(\eta - \eta_0) - 1] \right\}$$

(10.113a)

$$\varphi'(0 < \eta \leq \eta_0) = \frac{1}{m\eta_0} \left(1 + \frac{1}{m} \right) \left(\frac{\eta}{\eta_0} \right)^{(1-m)/m} \left(1 - \frac{\eta}{\eta_0} \right)$$

(10.113b)

The Reynolds shear stress vanishes at the solid boundary. Equation (10.113b) cannot be applicable to the very thin viscous sublayer in the vicinity of the boundary, where viscous shear stress prevails. Using the experimental data, Dey et al. (2010) estimated the values of coefficients and exponents as $\hat{x}_0 = 11.34$, $\beta = 0.078$, $\beta_1 = 3.17$, $\alpha = 0.455$, $\alpha_1 = -0.045$, $\eta_0 = 0.3$, $m = 6$, and $\xi = 79.87$.
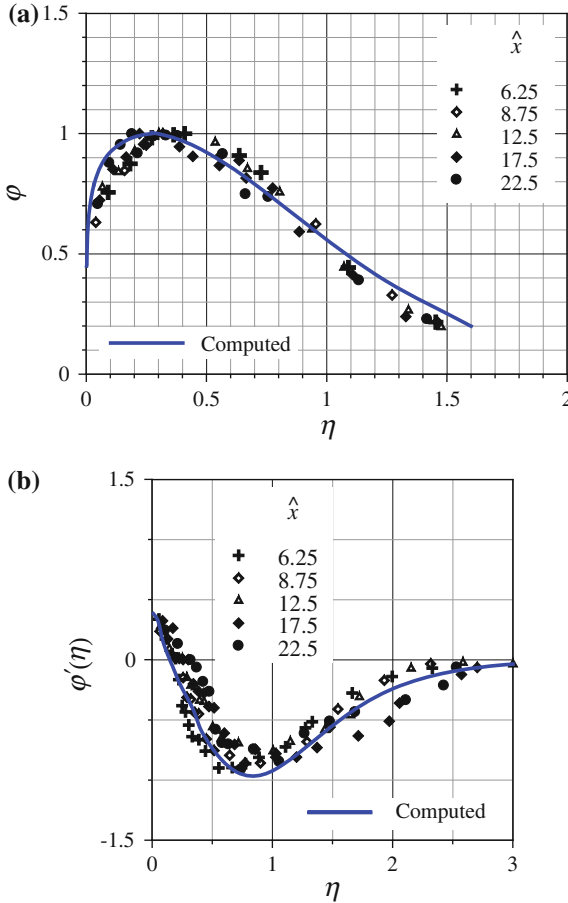
Fig. 10.31 **a** φ as a function of η and **b** φ' as a function of η for $U = 0.639$ m s^{-1} and $b_0 = 40$ mm in submerged plane wall jet (Dey et al. 2010)

Figures 10.31a, b show $\varphi(\eta)$ and $\varphi'(\eta)$ curves for $U = 0.639$ m s^{-1} and $b_0 = 40$ mm and the comparisons with the experimental data.

10.8.2 Computation of Scour Due to Submerged Wall Jets

The bed shear stress can be determined from Eq. (10.113b) by applying it to the near-bed level. In case of an erodible sediment bed, the bed is initially horizontal (before scour), and the fluid jet flows in the direction parallel to the horizontal bed surface of sediment. The jet erodes the bed forming a scour hole as shown in Fig. 10.32. The scour profile can be calculated by considering the bed shear stress distribution along the surface of the bed. To determine the bed shear stress τ_0 in the
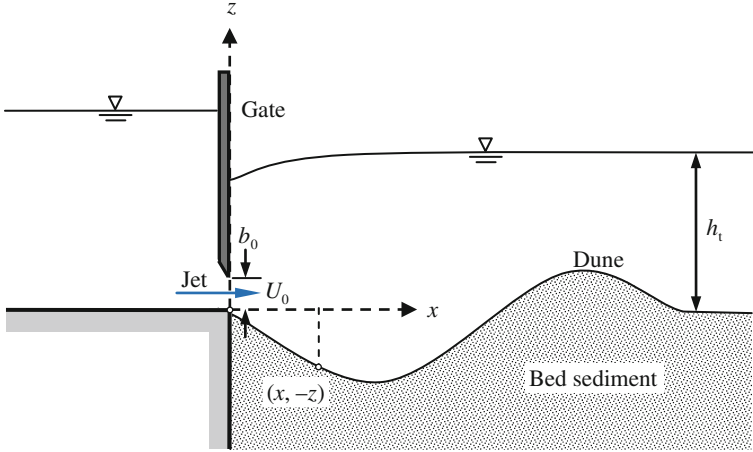
Fig. 10.32 Definition sketch of scour due to a submerged wall jet

scour hole, Eq. (10.113b) along with Eq. (10.112b) is thus applied to the particle level with an introduction to a shape function due to scour. With modification, the equation of bed shear stress τ_0 can then be given by

$$\tau_0(\hat{x}) = \rho U_0^2 \xi \, (\hat{x} + \hat{x}_0)^{-2\alpha} \frac{1}{m\eta_0} \left(1 + \frac{1}{m}\right) \left(\frac{\eta_b}{\eta_0}\right)^{(1-m)/m} \left(1 - \frac{\eta_b}{\eta_0}\right) G(\eta, \hat{x}) \quad (10.114)$$

where $\eta_b = k_s/\delta$ and $G(\eta, \hat{x})$ is a shape function to account for the bed shear stress variation when the bed is no longer horizontal. Here, k_s can be assumed as d_{50}. Note that the value of $\alpha = 0.5 + \alpha_1$ depends on submergence ratio S [$= (h_t - h_j)/h_j$], where h_j is the conjugate tailwater depth of free jump $\{= 0.5b_0[(1 + 8F_0^2)^{0.5} - 1]\}$ and F_0 is the jet Froude number [$= U_0/(gb_0)^{0.5}$].

Initially, the bed is horizontal ($\eta = 0$) and so $G(0, \hat{x}) = 1$. A Gaussian-like stress distribution with vertical distance can be assumed (Hogg el al. 1997):

$$G(\eta \geq 0, \hat{x}) = 1, \quad G(\eta < 0, \hat{x}) = \exp[(C_0\eta)^2] \quad (10.115)$$

where C_0 is the coefficient to be determined from the experimental data.

For equilibrium scour, Eq. (4.115) is reorganized as

$$\tau_0(\hat{x}) = \tau_{0c} \cos \theta \left(1 - \frac{\tan \theta}{\tan \phi}\right) \quad \wedge \quad \theta = \arctan\left(\frac{dz}{dx}\right) = \arctan\left(\hat{\delta}\frac{d\eta}{d\hat{x}}\right) \quad (10.116)$$

where $\hat{\delta} = \delta/b_0$. Using Eqs. (10.114) and (10.115), Eq. (10.116) which is a differential equation can be solved by Runge–Kutta method to determine the

variation of scour depth $\hat{z}(= \eta \hat{\delta})$ with $\hat{x}$, that is the nondimensional profile of equilibrium scour hole.

10.9 Examples

Example 10.1 Estimate the maximum equilibrium scour depth within a long contraction using the empirical equation given by Dey and Raikar for the following data:

Approaching flow depth, $h_1 = 5$ m
Approaching channel width, $B_1 = 70$ m
Channel width at contracted zone, $B_2 = 40$ m
Median size of sediment, $d_{50} = 2.6$ mm
Geometric standard deviation of sediment, $\sigma_g = 2.2$
Consider coefficient of kinematic viscosity of water $v = 10^{-6}$ m^2 s^{-1} and relative density of sediment $s = 2.65$

Solution

Use van Rijn's empirical formula for the determination of threshold shear velocity (see Table 4.1):

Particle parameter, $D_* = d_{50}(\Delta g/v^2)^{1/3} = 2.6 \times 10^{-3}\left[1.65 \times 9.81/\left(10^{-6}\right)^2\right]^{1/3}$
$= 65.77$
Threshold Shields parameter, $\Theta_c(20 < D_* \leq 150) = 0.013D_*^{0.29} = 0.013 \times 65.77^{0.29} = 0.044$
Threshold bed shear stress, $\tau_{0c} = \Theta_c \Delta \rho g d_{50} = 0.044 \times 1.65 \times 10^3 \times 9.81 \times 2.6 \times 10^{-3} = 1.852$ Pa
Threshold shear velocity, $u_{*c} = (\tau_{0c}/\rho)^{0.5} = (1.852/10^3)^{0.5} = 0.043$ m s^{-1}

The approaching flow velocity $U_1|_{U_2=U_{cr}}^{d_s=0}$ that corresponds to the threshold of sediment motion within contraction is estimated from the solution of Eqs. (10.20)–(10.22) as follows:

Eq. (10.20) $\Rightarrow 5 + \dfrac{1}{2 \times 9.81}\left(U_1|_{U_2=U_{cr}}^{d_s=0}\right)^2 = h_2 + \dfrac{1}{2 \times 9.81}\left(U_2|_{U_2=U_{cr}}^{d_s=0}\right)^2$

Eq. (10.21) $\Rightarrow U_1|_{U_2=U_{cr}}^{d_s=0} \times 5 \times 70 = U_2|_{U_2=U_{cr}}^{d_s=0} h_2 \times 40$

Eq. (10.22) $\Rightarrow \dfrac{U_2|_{U_2=U_{cr}}^{d_s=0}}{0.043} = 5.75 \log \dfrac{h_2}{2 \times 2.6 \times 10^{-3}} + 6$

Numerically solving above three equations, $U_1|_{U_2=U_{cr}}^{d_s=0} = 0.565$ m s^{-1}

The threshold velocity of approaching flow is determined as follows:

$$U_{cr} = 0.043 \left(5.75 \log \frac{5}{2 \times 2.6 \times 10^{-3}} + 6 \right) = 1 \text{ m s}^{-1}$$

Then, for $U_{1ec} = U_{cr} - U_1|_{U_2=U_{cr}}^{d_s=0} = 1 - 0.565 = 0.435 \text{ m s}^{-1}$,

$$F_{1ec} = \frac{U_{1ec}}{(\Delta g h_1)^{0.5}} = \frac{0.435}{(1.65 \times 9.81 \times 5)^{0.5}} = 0.048$$

Using $B_2/B_1 = 40/70 = 0.571$ and $d_{50}/h_1 = 2.6 \times 10^{-3}/5 = 5.2 \times 10^{-4}$ in Dey and Raikar's equation (Eq. 10.24), the $[d_s]_{max}$ is estimated as

$$\frac{[d_s]_{max}}{h_1} = 0.368 \times 0.048^{0.55} \times 0.571^{-1.26} \times (5.2 \times 10^{-4})^{-0.19} = 0.59$$
$$\Leftarrow \text{ Eq. } (10.24)$$

The maximum scour depth in uniform sediment is $[d_s]_{max} = 0.59h_1 = 0.59 \times 5$ $= 2.95$ m

For nonuniform sediment with $\sigma_g = 2.2$ for which $K_\sigma = 0.38$ (Fig. 10.3), the maximum equilibrium scour depth in nonuniform sediment is $[d_s]_{max} = 0.38 \times 2.95 = 1.121$ m.

Example 10.2 Calculate the equilibrium scour depth below a drop structure using the equations of various investigators for the following data:

Height between upstream and downstream water levels, $H = 1.5$ m
Tailwater depth, $h_t = 0.9$ m
Discharge per unit width, $q = 1.4 \text{ m}^2 \text{ s}^{-1}$
Angle of jet entering the tailwater, $\theta_j = 60°$
Thickness of jet at the tailwater level, $l_0 = 0.1$ m
Sediment size, $d_{90} = 32$ mm and $d_{95} = 38$ mm
Relative density of sediment, $s = 2.65$

Solution

Schoklitsch's equation

$$d_s = 0.52 \frac{1.4^{0.57} \times 1.5^{0.2}}{(32 \times 10^{-3})^{0.32}} - 0.9 = 1.155 \text{ m} \Leftarrow \text{Eq.} (10.26)$$

Kotoulas' equation

$$d_s = \frac{1.9}{9.81^{0.35}} \cdot \frac{1.4^{0.7} \times 1.5^{0.35}}{(38 \times 10^{-3})^{0.4}} - 0.9 = 3.71 \text{ m} \Leftarrow \text{Eq. (10.27)}$$

Fahlbusch's equation
Velocity of jet entering the tailwater, $U_0 = q/l_0 = 1.4/0.1 = 14 \text{ m s}^{-1}$
Assume $K_p = 3.5$ (for gravels)

$$d_s = 3.5 \left(\frac{1.4 \times 14}{9.81} \sin 60° \right)^{0.5} - 0.9 = 3.7 \text{ m} \Leftarrow \text{Eq. (10.28)}$$

Graf's equation

$$d_s = \frac{3.6}{1.65^{4/9} \times 9.81^{0.3}} \cdot \frac{1.4^{0.6} \times 1.5^{0.5}}{(32 \times 10^{-3})^{0.4}} - 0.9 = 7.726 \text{ m} \Leftarrow \text{Eq. (10.29)}$$

Eggenberger and Müller's equation

$$d_s = \frac{22.88}{15.849} \cdot \frac{1.4^{0.6} \times 1.5^{0.5}}{(32 \times 10^{-3})^{0.4}} - 0.9 = 7.673 \text{ m} \Leftarrow \text{Eq. (10.50)}$$

Example 10.3 Calculate the equilibrium scour depth downstream of a grade-control structure for the following data:

  Approaching flow depth, $h = 1.2$ m
  Drop height, $Z_p = 0.5$ m
  Discharge per unit width, $q = 1.55 \text{ m}^2 \text{ s}^{-1}$
  Angle of jet near the original bed level, $\theta_j = 55°$
  90 % finer size of sediment, $d_{90} = 4$ mm
  Angle of repose of sediment, $\phi = 40°$
  Relative density of sediment, $s = 2.65$

Solution

Bormann and Julien's equation is used to calculate equilibrium scour depth downstream of a grade-control structure.
Approaching flow velocity, $U_1 = q/h = 1.55/1.2 = 1.292 \text{ m s}^{-1}$

$$d_s = \left\{ 1.8 \left[\frac{\sin 40°}{\sin(40° + 55°)} \right]^{0.8} \frac{1.55^{0.6} \times 1.292 \times \sin 55°}{(1.65 \times 9.81)^{0.8}(4 \times 10^{-3})^{0.4}} \right\} - 0.5 = 1.213 \text{ m}$$
$$\Leftarrow \text{Eq. (10.32)}$$

Example 10.4 Calculate the equilibrium scour depth due to a horizontal jet issuing from a sluice gate opening using the equations of various investigators for the following data:

Height between upstream and downstream water levels, $H = 0.5$ m
Tailwater depth, $h_t = 2$ m
Discharge per unit width, $q = 1.6$ m^2 s^{-1}
Sluice gate opening, $b_0 = 0.5$ m
Sediment size, $d_{50} = 10$ mm and $d_{90} = 18$ mm
Angle of repose of sediment, $\phi = 42°$
Relative density of sediment, $s = 2.65$
Dune height, $\eta_d = 0.1h_t$

Solution

Use van Rijn's empirical formula for the determination of threshold shear velocity (see Table 4.1):

Particle parameter, $D_* = d_{50}(\Delta g/v^2)^{1/3} = 10 \times 10^{-3}[1.65 \times 9.81/(10^{-6})^2]^{1/3} = 252.95$

Threshold Shields parameter, $\Theta_c(D_* > 150) = 0.055$
Threshold bed shear stress, $\tau_{0c} = \Theta_c\Delta\rho gd_{50} = 0.055 \times 1.65 \times 10^3 \times 9.81 \times 10 \times 10^{-3} = 8.903$ Pa
Threshold shear velocity, $u_{*c} = (\tau_{0c}/\rho)^{0.5} = (8.903/10^3)^{0.5} = 0.094$ m s^{-1}

Qayoum's equation

$$d_s = \frac{2.78}{9.81^{0.2}} \cdot \frac{1.6^{0.4} \times 0.5^{0.22} \times 2^{0.4}}{(18 \times 10^{-3})^{0.22}} - 2 = 3.826 \text{ m} \Leftarrow \text{Eq. (10.44)}$$

Altinbilek and Basmaci's equation

Jet velocity, $U_0 = q/b_0 = 1.6/0.5 = 3.2$ m s^{-1}

$$d_s = 0.5\left(\frac{0.5}{10 \times 10^{-3}}\tan 42°\right)^{0.5}\left[\frac{3.2}{(1.65 \times 9.81 \times 0.5)^{0.5}}\right]^{1.5} = 4 \text{ m} \Leftarrow \text{Eq.(10.45)}$$

Breusers and Raudkivi's equation

$$d_s = 8 \times 10^{-3} \times 0.5\left(\frac{3.2}{0.094}\right)^2 = 4.636 \text{ m} \Leftarrow \text{Eq. (10.46)}$$

Haffmans' equation

Averaged velocity over dune, $U_{crest} = q/(h_t - 0.1h_t) = q/(0.9h_t) = 1.6/(0.9 \times 2) = 0.889$ m s^{-1}

Scour factor, $\lambda_s = 6.8$ for $d_{90} = 18$ mm

$$d_s = 0.5\frac{50}{6.8}\left(1 - \frac{0.889}{3.2}\right) = 2.655 \text{ m} \Leftarrow \text{Eq. (10.47)}$$

Eggenberger and Müller's equation

$$d_s = \frac{10.35}{15.849} \cdot \frac{1.6^{0.6} \times 0.5^{0.5}}{(18 \times 10^{-3})^{0.4}} - 2 = 1.053 \text{ m} \Leftarrow \text{Eq. (10.50)}$$

Example 10.5 Determine the equilibrium scour depth downstream of an apron of length $L_0 = 3$ m due to a horizontal jet issuing from a sluice gate opening for the data given in Example 10.4.

Solution

Shalash's equation

$$d_s = 0.61\frac{1.6^{0.6}(0.5 + 2)^{0.5}}{(18 \times 10^{-3})^{0.4}}\left(1.5\frac{0.5}{3}\right)^{0.6} - 2 = 0.776 \text{ m} \Leftarrow \text{Eq. (10.48)}$$

Dey and Sarkar's equation

$$d_s = 2.59 \times 0.5\left[\frac{3.2}{(1.65 \times 9.81 \times 10 \times 10^{-3})^{0.5}}\right]^{0.94}\left(\frac{0.5}{3}\right)^{0.37}\left(\frac{2}{0.5}\right)^{0.16}\left(\frac{10 \times 10^{-3}}{0.5}\right)^{0.25}$$

$$= 2.2 \text{ m} \Leftarrow \text{Eq. (10.49)}$$

Example 10.6 Calculate the equilibrium scour depth downstream of a hydraulic structure due to a combined overfall and submerged jet for the following data:

   Height between upstream and downstream water levels, $H = 1.2$ m
   Tailwater depth, $h_t = 1.5$ m
   Total discharge per unit width, $q = 1.6$ m^2 s^{-1}
   Discharge through sluice opening, $q_0 = 0.6q$
   Sediment size, $d_{90} = 12$ mm

Solution

Eggenberger and Müller's equation

Submerged jet discharge through sluice opening, $q_0 = 0.6q = 0.6 \times 1.6 = 0.96$ m^2 s^{-1}

Overfall discharge, $q_1 = q - q_0 = 1.6 - 0.96 = 0.64$ m^2 s^{-1}
Discharge ratio, $\hat{q} = q_1/q_0 = 0.64/0.96 = 0.67$

$$c_0 = 22.88 - \frac{10^3}{4.9\hat{q}^3 - 6.3\hat{q}^2 + 29\hat{q} + 64}$$

$$= 22.88 - \frac{10^3}{4.9 \times 0.67^3 - 6.3 \times 0.67^2 + 29 \times 0.67 + 64} = 10.7$$

$$d_s = \frac{10.7}{15.849} \cdot \frac{1.6^{0.6} \times 1.2^{0.5}}{(12 \times 10^{-3})^{0.4}} - 1.5 = 4.251 \text{ m} \Leftarrow \text{Eq. (10.50)}$$

Example 10.7 Given pipe diameter, $D = 1.2$ m; embedment, $e = 0.1$ m; porosity of sediment, $\rho_0 = 0.4$; and relative density of sediment, $s = 2.65$, what is the threshold velocity of scour underneath the submarine pipeline?

Solution

From Eq. (10.51)

$$U_{gcr}^2 = 0.025\Delta g(1 - \rho_0)D \exp\left(81\frac{e}{D}\right)^{0.5}$$

$$= 0.025 \times 1.65 \times 9.81(1 - 0.4)1.2 \times \exp\left(81\frac{0.1}{1.2}\right)^{0.5} = 3.915$$

Therefore, $U_{gcr} = 1.979$ m s^{-1}

Example 10.8 Compute the equilibrium scour depth below a 0.1 m diameter underwater pipeline, laid on a sediment bed of $d_{50} = 0.6$ mm in a laboratory flume, subjected to a steady flow velocity of 0.35 m s^{-1} having a flow depth of 0.4 m. Take coefficient of kinematic viscosity of water $v = 10^{-6}$ m^2 s^{-1} and mass density of water $\rho = 10^3$ kg m^{-3}.

Solution

Given data are as follows:
Pipe diameter, $D = 0.1$ m; flow velocity, $U = 0.35$ m s^{-1}; flow depth, $h = 0.4$ m; sediment size, $d_{50} = 0.6$ mm; kinematic viscosity of water, $v = 10^{-6}$ m^2 s^{-1}; and mass density of water, $\rho = 10^3$ kg m^{-3}

Use van Rijn's empirical formula for the determination of threshold bed shear stress (see Table 4.1):

Particle parameter, $D_* = d_{50}(\Delta g/v^2)^{1/3} = 0.6 \times 10^{-3}[1.65 \times 9.81/(10^{-6})^2]^{1/3} = 15.18$

Threshold Shields parameter, $\Theta_c(10 < D_* \le 20) = 0.04D_*^{-0.1} = 0.04 \times 15.18^{-0.1} = 0.03$

Threshold bed shear stress, $\tau_{0c} = \Theta_c \Delta \rho g d_{50} = 0.03 \times 1.65 \times 10^3 \times 9.81 \times 0.6 \times 10^{-3} = 0.291$ Pa

Estimation of scour depth by Chiew's method
Discharge per unit width, $q = Uh = 0.35 \times 0.4 = 0.14$ m^2 s^{-1}. Then, q_g is

$$q_g = 0.781 \times 0.14 \left(\frac{0.1}{0.4}\right)^{0.787} = 0.0367 \text{ m}^2 \text{ s}^{-1} \Leftarrow \text{Eq. (10.55)}$$

Chiew proposed to determine friction factor λ_D from the Moody diagram. It can however also be determined from the Colebrook–White equation (Eq. 3.55). Remembering that the Colebrook–White equation is an implicit equation, it is therefore preferred here to use Haaland's (1983) explicit equation that gives an approximate solution for the Colebrook–White equation and can be used as a substitute. The original Haaland's equation is given for a pipe flow case having an average flow velocity U with an internal pipe diameter D_i as

$$\frac{1}{\lambda_D^{0.5}} = -0.782 \ln \left[\left(\frac{k_s}{3.7 D_i}\right)^{1.1} + \frac{6}{Re}\right] \quad \wedge \quad Re = \frac{U D_i}{v}$$

In this case, for the pressurized flow beneath the pipeline, the scour depth d_s and the average gap velocity U_g are analogous to D_i and U, respectively. The roughness height k_s can be assumed as d_{50} (= 0.6 mm)
For the first trial, assume $d_s = 0.12$ m and then calculate the average gap velocity $U_g = q_g/d_s = 0.0367/0.12 = 0.306$ m s^{-1} and the Reynolds number $Re = U_g d_s/v = 0.306 \times 0.12/10^{-6} = 36{,}720$. The friction factor is determined from Haaland's equation as

$$\frac{1}{\lambda_D^{0.5}} = -0.782 \ln \left[\left(\frac{0.6 \times 10^{-3}}{3.7 \times 0.12}\right)^{1.1} + \frac{6}{36720}\right] \Rightarrow \lambda_D = 0.033$$

Thus, the bed shear stress in the scour hole beneath the pipeline is

$$\tau_0 = \frac{\lambda_D}{8} \rho U_g^2 = \frac{0.033}{8} \times 10^3 \times 0.306^2 \Rightarrow \tau_0 = 0.386 \text{ Pa} \quad \therefore \quad \tau_0 \neq \tau_{0c}$$

Following a trial-and-error method, the value of d_s that satisfies the condition $\tau_0 = \tau_{0c}$ (= 0.291 Pa) is 0.136 m. Therefore, the equilibrium scour depth d_s is 0.136 m.

Example 10.9 Calculate the maximum scour depth at a rectangular pier for the following data:

Pier width, $b = 2$ m
Pier length, $L = 8$ m
Approaching flow depth, $h = 8$ m
Discharge per unit width, $q = 12$ m^2 s^{-1}
Flow skewness, $\alpha = 15°$
Median size of sediment, $d_{50} = 0.9$ mm (uniform sediment)

Use (1) Melville and Coleman's method (2) HEC18 method and (3) Sheppard et al.'s method.

Also, determine the size of riprap stone for the scour countermeasure at the pier. Assume the riprap to be placed at the original bed level.

Solution

Approaching flow velocity, $U = q/h = 12/8 = 1.5$ m s^{-1}

(1) *Calculation of scour depth by Melville and Coleman's method*

The threshold shear velocity and threshold approaching flow velocity are as follows:

$$u_{*c}(0.1 \text{ mm} \leq d_{50} < 1 \text{ mm}) = 0.0115 + 0.0125 d_{50}^{1.4} = 0.0115 + 0.0125 \times 0.9^{1.4}$$
$$= 0.022 \text{ m s}^{-1}$$

$$U_{cr} = u_{*c} 5.75 \log\left(5.53 \frac{h}{d_{50}}\right) = 0.022 \times 5.75 \log\left(5.53 \frac{8}{0.9 \times 10^{-3}}\right)$$
$$= 0.593 \text{ m s}^{-1} \Leftarrow \text{Eq. (10.67)}$$

For uniform sediment, $U_a = U_{cr}$
Computation of K-factors is as follows:

1. For $b/h = 2/8 = 0.25 < 0.7$, $K_h = 2.4b = 2.4 \times 2 = 4.8$ m $\Leftarrow$ Eq. (10.65)
2. For $\dfrac{U - (U_a - U_{cr})}{U_{cr}} = \dfrac{1.5}{0.593} = 2.53 > 1$, $K_I = 1 \Leftarrow$ Eq. (10.66)
3. For $b/d_{50} = 2/(0.9 \times 10^{-3}) = 2222.2 > 25$, $K_d = 1 \Leftarrow$ Eq. (10.68)
4. For a rectangular pier (square nosed), $K_s = 1.1$ (Table 10.2)
5. For $b_p = L\sin\alpha + b\cos\alpha = 8 \times \sin15° + 2 \times \cos15° = 4$ m, $K_\alpha = \left(b_p/b\right)^{0.65}$
   $= (4/2)^{0.65} = 1.569 \Leftarrow$ Eq. (10.70)
6. For an equilibrium scour ($t = t_e$), $K_t = 1 \Leftarrow$ Eq. (10.71)

Then, the scour depth is

$$d_s = K_h K_I K_d K_s K_\alpha K_t = 4.8 \times 1 \times 1 \times 1.1 \times 1.569 \times 1 = 8.284 \text{ m} \Leftarrow \text{Eq. (10.64)}$$

(2) Calculation of scour depth by HEC18 method

Computation of K-factors is as follows:

1. For a rectangular pier, $K_s = 1.1$ (Table 10.2)
2. For $L/b = 8/2 = 4$ and $\alpha = 15°$, $K_\alpha = 1.5$ (Table 10.4)
3. For $Fr = 1.5/(9.81 \times 8)^{0.5} = 0.169$ and U ($= 1.5 \text{ m s}^{-1}$) $> U_{cr}$ ($= 0.593 \text{ m s}^{-1}$), the possible bedforms are small dunes (assumed). Thus, $K_{bed} = 1.1$ (Table 10.3)
4. For $d_{50} = 0.9 \text{ mm} < 2 \text{ mm}$, $K_a = 1 \Leftarrow$ Eq. (10.75a)

Then, the scour depth is

$$\frac{d_s}{b} = 2K_s K_\alpha K_{bed} K_a \left(\frac{h}{b}\right)^{0.35} Fr^{0.43} = 2 \times 1.1 \times 1.5 \times 1.1 \times 1 \left(\frac{8}{2}\right)^{0.35} 0.169^{0.43}$$

$$= 2.745 \Leftarrow \text{Eq. (10.74)}$$

$$d_s = 2 \times 2.745 = 5.49 \text{ m}$$

(3) Calculation of scour depth by Sheppard et al.'s method

The threshold shear velocity and threshold approaching flow velocity are calculated as follows:

$$u_{*c} = \left\{ 16.2 d_{50} \left[\frac{9.09 \times 10^{-6}}{d_{50}} - d_{50}(38.76 + 9.6 \ln d_{50}) - 0.005 \right] \right\}^{0.5}$$

$$= \sqrt{16.2 \times 0.9 \times 10^{-3} \left\{ \frac{9.09 \times 10^{-6}}{0.9 \times 10^{-3}} - 0.9 \times 10^{-3}[38.76 + 9.6 \ln(0.9 \times 10^{-3})] - 0.005 \right\}}$$

$$= 0.021 \text{ m s}^{-1}$$

$$\Re = \frac{u_{*c} d_{50}}{2.32 \times 10^{-7}} = \frac{0.021 \times 0.9 \times 10^{-3}}{2.32 \times 10^{-7}} = 81.47 \ (\Re > 70)$$

$$U_{cr} = u_{*c} 2.5 \ln\left(2.21 \frac{h}{d_{50}}\right) = 0.021 \times 2.5 \ln\left(2.21 \frac{8}{0.9 \times 10^{-3}}\right) = 0.519 \text{ m s}^{-1} \Leftarrow \text{Eq. (10.78b)}$$

The effective pier diameter is calculated as follows:

$$K_s = 0.86 + 0.97 \left| \alpha - \frac{\pi}{4} \right|^4 = 0.86 + 0.97 \left| 15 \times \frac{\pi}{180} - \frac{\pi}{4} \right|^4 = 0.933$$

$$b_e = K_s b_p = 0.933 \times 4 = 3.732 \text{ m}$$

The functions are calculated as follows:

$$f_1 = \tanh\left[\left(\frac{h}{b_e}\right)^{0.4}\right] = \tanh\left[\left(\frac{8}{3.732}\right)^{0.4}\right] = 0.876$$

$$f_3 = \frac{\dfrac{b_e}{d_{50}}}{0.4\left(\dfrac{b_e}{d_{50}}\right)^{1.2} + 10.6\left(\dfrac{b_e}{d_{50}}\right)^{-0.13}} = \frac{\dfrac{3.732}{0.9 \times 10^{-3}}}{0.4\left(\dfrac{3.732}{0.9 \times 10^{-3}}\right)^{1.2} + 10.6\left(\dfrac{3.732}{0.9 \times 10^{-3}}\right)^{-0.13}}$$

$$= 0.472$$

Then, the scour depth is calculated as follows:

For $5U_{cr} < 0.6(gh)^{0.5}$, $U_{peak} = 0.6(gh)^{0.5} = 0.6(9.81 \times 8)^{0.5} = 5.315$ m s^{-1}.

$\therefore U_{cr} \le U \le U_{peak}$

$$\frac{d_s}{b_e} = f_1\left[2.2\left(\frac{U - U_{cr}}{U_{peak} - U_{cr}}\right) + 2.5f_3\left(\frac{U_{peak} - U}{U_{peak} - U_{cr}}\right)\right]$$

$$= 0.876\left[2.2\left(\frac{1.5 - 0.519}{5.315 - 0.519}\right) + 2.5 \times 0.472\left(\frac{5.315 - 1.5}{5.315 - 0.519}\right)\right]$$

$$= 1.216 \Leftarrow \text{Eq. (10.77b)}$$

$$d_s = b_e \times 1.216 = 3.732 \times 1.216 = 4.538 \text{ m}$$

Calculation of riprap stone size

By HEC-23 formula:

$$d_{50r} = 0.346\frac{(KU)^2}{\Delta g} = 0.346\frac{(1.7 \times 1.5)^2}{1.65 \times 9.81} = 0.139 \text{ m} \Leftarrow \text{Eq. (10.89)}$$

Note: For a rectangular pier, $K = 1.7$

By Lauchlan's equation:

Placement depth, $z_r = 0$

$$d_{50r} = 0.3f_{SF}h\left(1 - \frac{z_r}{h}\right)^{2.75}Fr^{1.2} = 0.3 \times 1.1 \times 8\left(1 - \frac{0}{8}\right)^{2.75}0.169^{1.2} = 0.313 \text{ m}$$

$$\Leftarrow \text{Eq. (10.90)}$$

Note: $f_{SF} = 1.1$ is considered in the above calculation.

Example 10.10 Determine scour depth in the end of the second day for $q = 4$ m^2 s^{-1} and other data same as in Example 10.9.

Solution

Approaching flow velocity, $U = q/h = 4/8 = 0.5$ m s^{-1} $< U_{cr}$ (= 0.519 m s^{-1})
For $U/U_{cr} = 0.5/0.519 = 0.963 < 1$ (clear-water   scour), $K_I = 0.963$
$\Leftarrow$ Eq. (10.66)
For $h/b = 8/2 = 4 < 6$ and $U/U_{cr} = 0.963 > 0.4$, the time t_e to reach equilibrium is

$$t_e = 30.89 \frac{b}{U} \left(\frac{U}{U_{cr}} - 0.4 \right) \left(\frac{h}{b} \right)^{0.25} = 30.89 \frac{2}{0.5} \left(\frac{0.5}{0.519} - 0.4 \right) \left(\frac{8}{2} \right)^{0.25} = 98.4 \text{ days}$$
$\Leftarrow$ Eq. (10.72)

For $t = 2$ days, K_t is

$$K_t = \exp\left[-0.03 \left| \frac{U_{cr}}{U} \ln\left(\frac{t}{t_e} \right) \right|^{1.6} \right] = \exp\left[-0.03 \left| \frac{0.519}{0.5} \ln\left(\frac{2}{98.4} \right) \right|^{1.6} \right] = 0.755$$
$\Leftarrow$ Eq. (10.71)

Then, the scour depth is

$$d_s = K_h K_I K_d K_s K_\alpha K_t = 4.8 \times 0.962 \times 1 \times 1.1 \times 1.569 \times 0.755 = 6.017 \text{ m}$$
$\Leftarrow$ Eq. (10.64)

Example 10.11 Calculate the maximum scour depth at a circular pier for the following data:

Pier diameter, $b = 2.5$ m
Approaching flow depth, $h = 3.4$ m
Discharge per unit width, $q = 11.9$ m^2 s^{-1}
Sediment size, $d_{50} = 20$ mm, $d_{95} = 85$ mm and $d_{max} = 99$ mm

Use (1) Melville and Coleman's method and (2) HEC18 method.
   Also, determine the size of riprap stone for the scour countermeasure at the pier. Assume the riprap to be placed 0.5 m below the original bed level.

Solution

Approaching flow velocity, $U = q/h = 11.9/3.4 = 3.5$ m s^{-1}

(1) *Calculation of scour depth by Melville and Coleman's method*
The threshold shear velocity u_{*c} and threshold approaching flow velocities, U_{cr}, U_{cra}, and U_a are calculated as follows:

$$u_{*c}(1 \text{ mm} \le d_{50} < 100 \text{ mm}) = 0.0305 d_{50}^{0.5} - 6.5 \times 10^{-3} d_{50}^{-1}$$

$$= 0.0305 \times 20^{0.5} - 6.5 \times 10^{-3} \times 20^{-1} = 0.136 \text{ m s}^{-1}$$

$$d_{50a} = d_{max}/1.8 = 99/1.8 = 55 \text{ mm}$$

$$u_{*ca}(1 \text{ mm} \le d_{50} < 100 \text{ mm}) = 0.0305 d_{50a}^{0.5} - 6.5 \times 10^{-3} d_{50a}^{-1}$$

$$= 0.0305 \times 55^{0.5} - 6.5 \times 10^{-3} \times 55^{-1} = 0.226 \text{ m s}^{-1}$$

$$U_{cr} = u_{*c} 5.75 \log\left(5.53 \frac{h}{d_{50}}\right) = 0.136$$

$$\times 5.75 \log\left(5.53 \frac{3.4}{20 \times 10^{-3}}\right)$$

$$= 2.325 \text{ m s}^{-1} \Leftarrow \text{Eq. (10.67)}$$

$$U_{cra} = u_{*ca} 5.75 \log\left(5.53 \frac{h}{d_{50a}}\right) = 0.226$$

$$\times 5.75 \log\left(5.53 \frac{3.4}{55 \times 10^{-3}}\right)$$

$$= 3.293 \text{ m s}^{-1} \Leftarrow \text{Eq. (10.67)}$$

$$U_a = 0.8 U_{cra} = 0.8 \times 3.293 = 2.634 \text{ m s}^{-1}$$

Computation of K-factors is as follows:

1. For $b/h = 2.5/3.4 = 0.735$ $(0.7 \le b/h \le 5)$, $K_h = 2(hb)^{0.5} = 2(3.4 \times 2.5)^{0.5} = 5.831 \text{ m} \Leftarrow$ Eq. (10.65)
2. For $\dfrac{U - (U_a - U_{cr})}{U_{cr}} = \dfrac{3.5 - (2.634 - 2.325)}{2.325} = 1.372 > 1$, $K_I = 1 \Leftarrow$ Eq. (10.66)
3. For $b/d_{50a} = 2/(55 \times 10^{-3}) = 36.36 > 25$, $K_d = 1 \Leftarrow$ Eq. (10.68)
4. For a circular pier, $K_s = 1$ (Table 10.2)
5. For a circular pier, $K_\alpha = 1 \Leftarrow$ Eq. (10.70)
6. For an equilibrium scour $(t = t_e)$, $K_t = 1 \Leftarrow$ Eq. (10.71)

Then, the scour depth is

$$d_s = K_h K_I K_d K_s K_\alpha K_t = 5.831 \times 1 \times 1 \times 1 \times 1 \times 1 = 5.831 \text{ m} \Leftarrow \text{Eq. (10.64)}$$

(2) *Calculation of scour depth by HEC18 method*

$$U_{cr}|_{d_{50}} = 6.19h^{1/6}d_{50}^{1/3} = 6.19 \times 3.4^{1/6}(20 \times 10^{-3})^{1/3}$$
$$= 2.06 \text{ m s}^{-1} \Leftarrow \text{Eq. (10.76)}$$

$$U_{cr}|_{d_{95}} = 6.19h^{1/6}d_{95}^{1/3} = 6.19 \times 3.4^{1/6}(85 \times 10^{-3})^{1/3}$$
$$= 3.337 \text{ m s}^{-1} \Leftarrow \text{Eq. (10.76)}$$

$$U_{crs}|_{d_{50}} = 0.645\left(\frac{d_{50}}{b}\right)^{0.053} U_{cr}|_{d_{50}} = 0.645\left(\frac{20 \times 10^{-3}}{2}\right)^{0.053} 2.06$$
$$= 1.041 \text{ m s}^{-1} \Leftarrow \text{Eq. (10.76)}$$

$$U_{crs}|_{d_{95}} = 0.645\left(\frac{d_{95}}{b}\right)^{0.053} U_{cr}|_{d_{95}} = 0.645\left(\frac{85 \times 10^{-3}}{2}\right)^{0.053} 3.337$$
$$= 1.821 \text{ m s}^{-1} \Leftarrow \text{Eq. (10.76)}$$

$$U_{r} = \frac{U - U_{crs}|_{d_{50}}}{U_{cr}|_{d_{50}} - U_{crs}|_{d_{95}}} = \frac{3.5 - 1.041}{2.06 - 1.821} = 10.289 \Leftarrow \text{Eq. (10.75b)}$$

Computation of *K*-factors is as follows:

1. For a circular pier, $K_s = 1$ (Table 10.2)
2. For a circular pier, $K_\alpha = 1$
3. For $Fr = 3.5/(9.81 \times 3.4)^{0.5} = 0.6$ and U (= 3.5 m s^{-1}) > U_{cr} (= 2.06 m s^{-1}), the possible bedforms are large dunes (assumed). Thus, $K_{bed} = 1.3$ (Table 10.3)
4. For $d_{50} = 20$ mm > 2 mm and $d_{95} = 85$ mm > 20 mm, $K_a = 0.4U_r^{0.15} = 0.4 \times 10.289^{0.15} = 0.567 \Leftarrow$ Eq. (10.75b)

Then, the scour depth is

$$\frac{d_s}{b} = 2K_s K_\alpha K_{bed} K_a \left(\frac{h}{b}\right)^{0.35} Fr^{0.43} = 2 \times 1 \times 1 \times 1.3 \times 0.567\left(\frac{3.4}{2.5}\right)^{0.35} 0.6^{0.43}$$
$$= 1.318 \Leftarrow \text{Eq. (10.74)}$$
$$d_s = 2.5 \times 1.318 = 3.295 \text{ m}$$

Calculation of riprap stone size
By HEC-23 formula:

$$d_{50r} = 0.346\frac{(KU)^2}{\Delta g} = 0.346\frac{(1.5 \times 3.5)^2}{1.65 \times 9.81} = 0.589 \text{ m} \Leftarrow \text{Eq. (10.89)}$$

Note: For a circular pier, $K = 1.5$
By Lauchlan's equation:
Placement depth, $z_r = 0.5$ m

$$d_{50r} = 0.3 f_{SF} h \left(1 - \frac{z_r}{h}\right)^{2.75} Fr^{1.2} = 0.3 \times 1.5 \times 3.4 \left(1 - \frac{0.5}{3.4}\right)^{2.75} 0.6^{1.2} = 0.535 \text{ m}$$
$$\Leftarrow \text{Eq. (10.90)}$$

Note: $f_{SF} = 1.5$ is considered in the above calculation.

Example 10.12 Calculate the maximum scour depth at a spill-through abutment for the following data:

   Abutment length $= 10$ m
   Abutment length spanning to flood channel $= 95$ % of abutment length
   Abutment slope, $S_a = 0.5$ (horizontal) : 1 (vertical)
   Abutment alignment, $\alpha = 80°$
   Flow depth in main channel, $h_m = 8$ m
   Flow depth in flood channel, $h^* = 2$ m
   Discharge per unit width in main channel, $q = 20$ m^2 s^{-1}
   Discharge per unit width in flood channel, $q^* = 5$ m^2 s^{-1}
   Manning coefficient in main channel, $n = 0.022$ SI units
   Manning coefficient in flood channel, $n^* = 0.03$ SI units
   Sediment size, $d_{50} = 20$ mm, $d_{95} = 85$ mm, and $d_{max} = 99$ mm

Assume the flow depth reduction to be 2 % in the contracted portion.
   Use (1) Melville and Coleman's method and (2) HEC18 method.
   Also, determine the size of riprap stone for scour countermeasure at the abutment.

Solution

Calculation is based on the flow in the flood channel, where 95 % of abutment length exists.
Approaching flow velocity in flood channel, $U = q^*/h^* = 5/2 = 2.5$ m s^{-1}
Projected abutment length, $l = 10 \sin\alpha = 10 \sin80° = 9.848$ m
Projected abutment length in flood channel, $l^* = 10 \times 0.95 \sin\alpha = 10 \times 0.95 \sin80° = 9.356$ m
The threshold approaching flow velocities, U_{cr}, U_{cra}, and U_a, are as follows:
   $u_{*c} = 0.136$ m s^{-1}; $u_{*ca} = 0.226$ m s^{-1}; $d_{50a} = 55$ mm (see Example 10.11)

$$U_{cr} = u_{*c} 5.75 \log\left(5.53 \frac{h^*}{d_{50}}\right) = 0.136 \times 5.75 \log\left(5.53 \frac{2}{20 \times 10^{-3}}\right)$$
$$= 2.145 \text{ m s}^{-1} \Leftarrow \text{Eq. (10.67)}$$
$$U_{cra} = u_{*ca} 5.75 \log\left(5.53 \frac{h^*}{d_{50a}}\right) = 0.226 \times 5.75 \log\left(5.53 \frac{2}{55 \times 10^{-3}}\right)$$
$$= 2.993 \text{ m s}^{-1} \Leftarrow \text{Eq. (10.67)}$$
$$U_a = 0.8 U_{cra} = 0.8 \times 2.993 = 2.394 \text{ m s}^{-1}$$

Calculation of scour depth by Melville and Coleman's method
Computation of *K*-factors is as follows:

1. For $l/h^* = 9.848/2 = 4.924$ ($1 \le l/h^* \le 25$), $K_h = 2(h^*l)^{0.5} = 2(2 \times 9.848)^{0.5}$
   $= 8.876$ m $\Leftarrow$ Eq. (10.80)

Note: As the flow depth in flood channel is applicable, h is replaced by h^* in Eq. (10.80)

2. For $\dfrac{U - (U_a - U_{cr})}{U_{cr}} = \dfrac{2.5 - (2.394 - 2.145)}{2.145} = 1.049 > 1$, $K_I = 1 \Leftarrow$ Eq.(10.66)

3. For $l/d_{50a} = 9.848/(55 \times 10^{-3}) = 179.05 > 25$, $K_d = 1 \Leftarrow$ Eq. (10.81)

4. For a spill-through abutment with slope $S_a = 0.5{:}1$, $K_s = 0.6$ (Table 10.6)

5. For $\alpha = 80°$, $K_\alpha^* = 0.993$ is obtained from Table 10.7. Then, for $l/h^* = 4.924 > 3$, $K_\alpha = 0.993 \Leftarrow$ Eq. (10.83)

6. K_G is calculated, considering $h = h_m$, that is, the flow depth in main channel, as

$$
K_G = \left\{ 1 - \left(\frac{l^*}{l} \right) \left[1 - \left(\frac{h^*}{h} \right)^{5/3} \left(\frac{n}{n^*} \right) \right] \right\}^{0.5}
$$

$$
= \left\{ 1 - \left(\frac{9.356}{9.848} \right) \left[1 - \left(\frac{2}{8} \right)^{5/3} \left(\frac{0.022}{0.03} \right) \right] \right\}^{0.5} = 0.345 \Leftarrow \text{Eq. (10.84)}
$$

7. For an equilibrium scour ($t = t_e$), $K_t = 1 \Leftarrow$ Eq. (10.85)

Then, the scour depth is
   $d_s = K_h K_I K_d K_s K_\alpha K_G K_t = 8.876 \times 1 \times 1 \times 0.6 \times 0.993 \times 0.345 \times 1 = 1.824$ m
   $\Leftarrow$ Eq.(10.79)

Calculation of riprap stone size
By Austroads formula:
   $Fr = U/(gh^*)^{0.5} = 2.5/(9.81 \times 2)^{0.5} = 0.564$

$$
d_{50r} = 1.026 \frac{h^* Fr^2}{\Delta} = 1.026 \frac{2 \times 0.564^2}{1.65} = 0.396 \text{ m} \Leftarrow \text{Eq. (10.91)}
$$

By Lauchlan's equation:
Shape factor, $K_s = 0.89$
Flow depth in contracted portion, $h_2 = 8 - 0.02 \times 8 = 7.84$ m
Flow velocity in contracted portion, $U_2 = q/h_2 = 20/7.84 = 2.551$ m s^{-1}
Froude number in contracted portion, $Fr_2 = U_2/(gh_2)^{0.5} = 2.551/(9.81 \times 7.84)^{0.5}$
$= 0.291 < 0.8$

$$
d_{50r} = K_s \frac{h_2 Fr_2^2}{\Delta} = 0.89 \frac{7.84 \times 0.291^2}{1.65} = 0.358 \text{ m} \Leftarrow \text{Eq. (10.92a)}
$$

Example 10.13 Determine scour depth in the end of the second day for the discharge per unit width in flood channel $q = 4 \text{ m}^2 \text{ s}^{-1}$ and other data same as in Example 10.12.

Solution

Approaching flow velocity in flood channel, $U = q^*/h^* = 4/2 = 2 \text{ m s}^{-1}$

For $\dfrac{U - (U_a - U_{cr})}{U_{cr}} = \dfrac{2 - (2.394 - 2.145)}{2.145} = 0.816 < 1$, $K_I = 0.816 \Leftarrow$ Eq. (10.66)

For $l/h^* = 9.848/2 = 4.924 > 1.2$, the time t_e to reach equilibrium is

$$t_e = 25\frac{h}{U} = 25\frac{2}{2} = 25 \text{ days} \Leftarrow \text{Eq. (10.86)}$$

For $t = 2$ days, K_t is

$$K_t = 0.1\frac{U_{cr}}{U}\ln\left(\frac{t}{t_e}\right) + 1 = 0.1\frac{2.145}{2}\ln\left(\frac{2}{25}\right) + 1 = 0.729 \Leftarrow \text{Eq. (10.85)}$$

Then, the scour depth is

$$d_s = K_h K_I K_d K_s K_\alpha K_G K_t = 8.876 \times 0.816 \times 1 \times 0.6 \times 0.993 \times 0.345 \times 0.729$$
$$= 1.085 \text{ m} \Leftarrow \text{Eq. (10.79)}$$

Example 10.14 Calculate the maximum scour depth at a vertical-wall abutment for the following data:

Abutment length, $l = 12$ m
Abutment alignment, $\alpha = 90°$
Flow depth, $h = 8$ m
Discharge per unit width, $q = 24 \text{ m}^2 \text{ s}^{-1}$
Median size of sediment, $d_{50} = 0.9$ mm (uniform sediment)

Solution

Approaching flow velocity, $U = q/h = 24/8 = 3 \text{ m s}^{-1}$
Threshold approaching flow velocity, $U_{cr} = 0.593 \text{ m s}^{-1}$ (see Example 10.9)
It is a live-bed flow condition ($U > U_{cr}$). Hence, Froehlich's (HEC 18) method is applicable

Calculation of scour depth by HEC18 method:
Computation of K-factors is as follows:
Flow Froude number, $Fr = U/(gh)^{0.5} = 3/(9.81 \times 8)^{0.5} = 0.339$

1. For a vertical-wall abutment, $K_s = 1$ (Table 10.8)
2. For $\alpha = 90°$, $K_\alpha = 1 \Leftarrow$ Eq. (10.88)

Then, the scour depth is

$$\frac{d_s}{l} = 2.27 K_s K_\alpha \left(\frac{h}{l}\right)^{0.57} Fr^{0.61} + 1 = 2.27 \times 1 \times 1 \left(\frac{8}{12}\right)^{0.57} 0.339^{0.61} + 1$$

$$= 1.931 \Leftarrow \text{Eq. (10.87)}$$

$$d_s = 12 \times 1.931 = 23.172 \text{ m}$$

References

Altinbilek HD, Basmaci Y (1973) Localized scour at the downstream of outlet structures. In: Proceedings of the eleventh congress on Large Dam, Madrid, pp 105–121

Atayee AT, Pagan-Ortiz JE, Jones JS, Kilgore RT (1993) A study of riprap as a scour protection for spill-through abutments. American Society of Civil Engineers (ASCE) hydraulic engineering conference, San Francisco, California

Austroads (1994) Waterway design—a guide to the hydraulic design of bridges, culverts and floodways. Austroads, Sydney

Bakhmeteff BA (1932) Hydraulics of open channels. McGraw-Hill, New York

Barbhuiya AK (2003) Clear water scour at abutments. PhD thesis, Department of Civil Engineering, Indian Institute of Technology, Kharagpur

Barbhuiya AK, Dey S (2004) Velocity and turbulence at a wing-wall abutment. Proc Indian Acad Sci Sadhana 29(Feb):35–56

Barenblatt GI, Chorin AJ, Prostokishin VM (2005) The turbulent wall jet: a triple-layered structure and incomplete similarity. Proc Natl Acad Sci 102(25):8850–8853

Bijker EW, Leeuwestein W (1984) Interaction between pipeline and the seabed under the influence of waves and current. In: Proceedings of the symposium of International Union of Theoretical and Applied Mechanics/International Union of Geology and Geophysics, seabed mechanics, pp 235-242

Bormann NE, Julien PY (1991) Scour downstream of grade-control structures. J Hydraul Eng 117(5):579–594

Breusers HNC, Nicollet G, Shen HW (1977) Local scour around cylindrical piers. J Hydraul Res 15(3):211–252

Breusers HNC, Raudkivi AJ (1991) Scouring. Balkema, Rotterdam

Chao JL, Hennessy PV (1972) Local scour under ocean outfall pipe-lines. J Water Pollut Control Fed 44(7):1443–1447

Chiew YM (1991) Prediction of maximum scour depth at submarine pipelines. J Hydraul Eng 117(4):452–466

Chiew YM (1995) Mechanics of riprap failure at bridge piers. J Hydraul Eng 121(9):635–643

Chiew YM, Lim SY (2003) Protection of bridge piers using a sacrificial sill. Water Marit Energ Proc Inst Civ Eng (London) 156(1):53–62

Croad RN (1997) Protection from scour of bridge piers using riprap. Transit New Zealand research report number PR3-0071, Works Consultancy Services Limited, Central Laboratories, Lower Hutt, Wellington

D'Agostino V, Ferro V (2004) Scour on alluvial bed downstream of grade-control structures. J Hydraul Eng 130(1):24–37

Dey S (1991) Clear water scour around circular bridge piers: a model. PhD thesis, Department of Civil Engineering, Indian Institute of Technology, Kharagpur

Dey S (1995) Three-dimensional vortex flow field around a circular cylinder in a quasi-equilibrium scour hole. Proc Indian Acad Sci Sadhana 20(Dec):871–885

Dey S (1997a) Local scour at piers, part 1: a review of development of research. Int J Sediment Res 12(2):23–44

Dey S (1997b) Local scour at piers, part 2: bibliography. Int J Sediment Res 12(2):45–57

Dey S (1999) Time-variation of scour in the vicinity of circular piers. Water Marit Energ Proc Inst Civ Eng (London) 136(2):67–75

Dey S, Barbhuiya AK (2004) Clear water scour at abutments. Water Management Proc Inst Civ Eng (London) 157(WM2):77–97

Dey S, Barbhuiya AK (2005a) Turbulent flow field in a scour hole at a semicircular abutment. Can J Civ Eng 32(1):213–232

Dey S, Barbhuiya AK (2005b) Flow field at a vertical-wall abutment. J Hydraul Eng 131(12):1126–1135

Dey S, Barbhuiya AK (2006) 3D flow field in a scour hole at a wing-wall abutment. J Hydraul Res 44(1):33–50

Dey S, Bose SK (1994) Bed shear in equilibrium scour around a circular cylinder embedded in loose bed. Appl Math Model 18(5):265–273

Dey S, Bose SK, Sastry GLN (1995) Clear water scour at circular piers: a model. J Hydraul Eng 121(12):869–876

Dey S, Nath TK, Bose SK (2010) Submerged wall jets subjected to injection and suction from the wall. J Fluid Mech 653:57–97

Dey S, Raikar RV (2005) Scour in long contractions. J Hydraul Eng 131(12):1036–1049

Dey S, Raikar RV (2006) Live-bed scour in long contractions. Int J Sediment Res 21(2):166–170

Dey S, Raikar RV (2007a) Characteristics of horseshoe vortex in developing scour holes at piers. J Hydraul Eng 133(4):399–413

Dey S, Raikar RV (2007b) Scour below a high vertical drop. J Hydraul Eng 133(5):564–568

Dey S, Sarkar A (2006a) Scour downstream of an apron due to submerged horizontal jets. J Hydraul Eng 132(3):246–257

Dey S, Sarkar A (2006b) Response of velocity and turbulence in submerged wall jets to abrupt changes from smooth to rough beds and its application to scour downstream of an apron. J Fluid Mech 556:387–419

Dey S, Singh NP (2007) Clear-water scour depth below underwater pipelines. J Hydro-Environ Res 1(2):157–162

Dey S, Singh NP (2008) Clear-water scour below underwater pipelines under steady flow. J Hydraul Eng 134(5):588–600

Dey S, Sumer BM, Fredsøe J (2006) Control of scour at vertical circular piles under waves and current. J Hydraul Eng 132(3):270–279

Eggenberger W, Müller R (1944) Experimentelle und theoretische untersuchunger über das kolkproblem. Number 5, Mitteilungen der Versuchsanstalt für Wasserbau, ETH Zurich, Zurich

Ettema R (1980) Scour at bridge piers. Report number 216, School of Engineering, University of Auckland, Auckland

Fahlbusch FE (1994) Scour in rock riverbeds downstream of large dams. Int J Hydropower Dams 1(4):30–32

Fredsøe J, Deigaard R (1992) Mechanics of coastal sediment transport. World Scientific, Singapore

Froehlich DC (1989) Local scour at bridge abutments. In: Proceedings of the national conference on hydraulic engineering, American Society of Civil Engineers, New Orleans, LA, pp 13–18

Gaudio R, Marion A (2003) Time evolution of scouring downstream of bed sills. J Hydraul Res 41(3):271–284

Gaudio R, Marion A, Bovolin V (2000) Morphological effects of bed sills in degrading rivers. J Hydraul Res 38(2):89–96

Gill MA (1970) Bed erosion around obstructions in rivers. PhD thesis, University of London, London

Gill MA (1972) Erosion of sand beds around spur-dikes. J Hydraul Div 98(9):1587–1602

Gill MA (1981) Bed erosion in rectangular long constriction. J Hydraul Div 107(3):273–284

Graf WH (1998) Fluvial hydraulics: flow and transport processes in channels of simple geometry. Wiley, Chichester

Graf WH, Istiarto I (2002) Flow pattern in the scour hole around a cylinder. J Hydraul Res 40(1):13–20

Grimaldi C, Gaudio R, Calomino F, Cardoso AH (2009) Countermeasures against local scouring at bridge piers: slot and combined system of slot and bed sill. J Hydraul Eng 135(5):425–431

Haaland SE (1983) Simple and explicit formulas for the friction factor in turbulent flow. J Fluids Eng 105(5):89–90

Hancu S (1971) Sur le calcul des affouillements locaux dans la zone des piles du pont. In: Proceedings of the fourteenth congress of International Association for Hydraulic Research, Paris, pp 299–305

Haque MA, Rahman MM, Islam GMT, Hussain MA (2007) Scour mitigation at bridge piers using sacrificial piles. Int J Sediment Res 22(1):49–59

Hoffmans GJCM (1998) Jet scour in equilibrium phase. J Hydraul Eng 124(4):430–437

Hoffmans GJCM, Verheij HC (1997) Scour manual. Balkema, Rotterdam

Hogg AJ, Huppert HE, Dade WB (1997) Erosion by planar turbulent wall jets. J Fluid Mech 338:317–340

Ibrahim A, Nalluri C (1986) Scour prediction around marine pipelines. In: Proceedings of the fifth international symposium on offshore mechanics and arctic engineering, Tokyo, pp 679–684

Isbash SV (1936) Construction of dams by depositing rock in running water. In: Transactions of the second congress on Large Dams, vol 5. Washington DC, pp 126–136

Jain SC (1981) Maximum clear-water scour around circular piers. J Hydraul Div 107(5):611–626

Jain SC, Fischer EE (1979) Scour around bridge piers at high Froude numbers. Report number FHWA-RD-79-104, Federal Highway Administration, US Department of Transportation, Washington DC

Jain SC, Fischer EE (1980) Scour around bridge piers at high flow velocities. J Hydraul Div 106(11):1827–1841

Jensen BL, Sumer BM, Jensen R, Fredsøe J (1990) Flow around and forces on a pipeline near scoured bed in steady current. J Offshore Mech Arct Eng 112(3):206–213

Kandasamy JK, Melville BW (1998) Maximum local scour depth at bridge piers and abutments. J Hydraul Res 36(2):183–198

Kim UY, Kim JS, Ahn SJ, Hahm CH (2005) Scour countermeasure using additional facility in front of bridge pier. In: Proceedings of the thirty-first congress of International Association for Hydraulic Research, Seoul, pp 5823–5829

Kjeldsen SP, Gjørsvik O, Bringaker KG, Jacobsen J (1973) Local scour near offshore pipelines. In: Proceedings of the second international conference on port and ocean engineering under arctic conditions, University of Iceland, Iceland, pp 308–331

Komura S (1966) Equilibrium depth of scour in long constrictions. J Hydraul Div 92(5):17–37

Kotoulas D (1967) Das kolkproblem unter besonderer berücksichtigung der faktoren zeit und geschiebemischung im rahmen der wildbachverbauung. Dissertation, Technischen Hochschule Zürich, Zürich

Kwan TF (1988) A study of abutment scour. Report number 451, School of Engineering, University of Auckland, Auckland

Kwan TF, Melville BW (1994) Local scour and flow measurements at bridge abutments. J Hydraul Res 32(5):661–673

Lagasse PF, Clopper PE, Zevenbergen LW, Girard LG (2007) Countermeasures to protect bridge piers from scour. NCHRP report 593, Transportation Research Board, Washington DC

Lagasse PF, Zevenbergen LW, Schall JD, Clopper PE (2001) Bridge scour and stream instability countermeasures. Hydraulic engineering circular number 23 (HEC 23), Publication number NHI 01-003, Federal Highway Administration, Washington DC

Lauchlan CS (1999) Pier scour countermeasures. PhD thesis, University of Auckland, Auckland

Launder BE, Rodi W (1981) The turbulent wall jet. Prog Aerosp Sci 19(2–4):81–128

Laursen EM (1963) An analysis of relief bridge scour. J Hydraul Div 89(3):93–118

Laursen EM, Toch A (1956) Scour around bridge piers and abutments. Bulletin number 4, Iowa Highways Research Board, Ames, Iowa

Lenzi MA, Marion A, Comiti F, Gaudio R (2002) Local scouring in low and high gradient streams at bed sills. J Hydraul Res 40(6):731–739

Lim S-Y (1993) Clear water scour in long contractions. Water Marit Energ Proc Inst Civ Eng (London) 101(2):93–98

Lim S-Y (1997) Equilibrium clear-water scour around an abutment. J Hydraul Eng 123(3):237–243

Lim S-Y, Cheng N-S (1998) Scouring in long contractions. J Irrig Drainage Eng 124(5):258–261

Liu HK, Chang FM, Skinner M (1961) Effect of bridge construction on scour and backwater. CER 60 HKL 22, Colorado State University, Civil Engineering Section, Fort Collins, Colorado

Macky GH (1990) Survey of roading expenditure due to scour. Report 90.09, Department of Scientific and Industrial Research, Hydrology Centre, Christchurch

Melville BW (1975) Local scour at bridge sites. Report number 117, School of Engineering, University of Auckland, Auckland

Melville BW (1992) Local scour at bridge abutments. J Hydraul Eng 118(4):615–631

Melville BW, Coleman SE (2000) Bridge scour. Water Resources Publications, Fort Collins

Melville BW, Hadfield AC (1999) Use of sacrificial piles as pier scour countermeasures. J Hydraul Eng 125(11):1221–1224

Melville BW, Parola AC, Coleman SE (2008) Bridge-scour prevention and countermeasures. In: García MH (ed) Sedimentation engineering: processes, measurements, modeling, and practice, ASCE manuals and reports on engineering practice number 110, American Society of Civil Engineers, Reston, VA, pp 543–577

Melville BW, Sutherland AJ (1988) Design method for local scour at bridge piers. J Hydraul Eng 114(10):1210–1226

Moncada-M A, Aguirre-Pe J (1999) Scour below pipeline in river crossings. J Hydraul Eng 125(9):953–958

Neill CR (1964) River bed scour, a review for bridge engineers. Contract number 281, Research Council of Alberta, Calgary, Alberta

Neill CR (1973) Guide to bridge hydraulics. University of Toronto Press, Toronto (Roads and Transportation Association of Canada)

Odgaard AJ, Wang Y (1991) Sediment management with submerged vanes 1: theory. J Hydraul Eng 117(3):267–283

Parker G, Toro-Escobar C, Voigt RL (1998) Countermeasures to protect bridge piers from scour. Final report NCHRP project 24-7, Transportation Research Board, Washington DC

Parola AC (1995) Boundary stress and stability of riprap at bridge piers. In: Thorne CR, Abt SR, Barends FBJ, Maynord ST, Pilarczyk KW (eds) River, coastal and shoreline protection: erosion control using riprap and armor stone. Wiley, Chichester, pp 149–158

Qayoum A (1960) Die gesetzmäßigkeit der kolkbildung hinter unterströmter wehren unter spezieller berücksichtigung der gestaltung eines beweglichen sturzbettes. Dissertation, Technischen Hochschule Carolo-Wilhelmina, Braunschweig

Raikar RV, Dey S (2005a) Scour of gravel beds at bridge piers and abutments. Water Management Proc Inst Civil Eng (London) 158(Jun):157–162

Raikar RV, Dey S (2005b) Clear-water scour at bridge piers in fine and medium gravel beds. Can J Civ Eng 32(4):775–781

Raikar RV, Dey S (2008) Kinematics of horseshoe vortex development in an evolving scour hole at a square cylinder. J Hydraul Res 46(2):247–264

Rajaratnam N (1976) Turbulent jets. Elsevier Science, Amsterdam

Raudkivi AJ (1986) Functional trends of scour bridge piers. J Hydraul Eng 112(1):1–13

Richardson EV, Davis SR (2001) Evaluating scour at bridges. Hydraulic engineering circular number 18 (HEC 18). Publication number NHI 01-001, Federal Highway Administration, US Department of Transportation, Washington DC

Richardson EV, Harrison LJ, Richardson JR, Davis SR (1993) Evaluating scour at bridges. Publication number FHWA-IP-90-017, Federal Highway Administration, US Department of Transportation, Washington DC

Rouse H (1936) Discharge characteristics of the free overfall. Civ Eng 6(4):125–134

Schlichting H (1979) Boundary layer theory. McGraw-Hill Book Company, New York

Schoklitsch A (1932) Kolkbildung unter uberfallstrahlen. Wasserwirtschaft 24:341–343

Schwarz WH, Cosart WP (1961) The two-dimensional turbulent wall jet. J Fluid Mech 10:481–495

Shalash MSE (1959) Die kolkbildung beim ausfluss unter schützen. Dissertation, Technischen Hochschule München, Munich

Shen HW, Schneider VR, Karaki S (1969) Local scour around bridge piers. J Hydraul Div 95(6):1919–1940

Sheppard DM, Melville B, Demir H (2014) Evaluation of existing equations for local scour at bridge piers. J Hydraul Eng 140(1):14–23

Smith CD (1967) Simplified design for flume inlets. J Hydraul Div 93(6):25–34

Stein OR, Julien PY, Alonso CV (1993) Mechanics of jet scour downstream of a headcut. J Hydraul Res 31(6):723–738

Straub LG (1934) Effect of channel contraction works upon regimen of movable bed streams. Trans Am Geophys Union 15(2):454–463

Sturm TW, Janjua NS (1994) Clear water scour around abutments in floodplains. J Hydraul Eng 120(8):956–972

Sumer BM, Fredsøe J (2002) The mechanism of scour in the marine environment. World Scientific, Singapore

Sumer BM, Truelsen C, Sichmann T, Fredsøe J (2001) Onset of scour below pipelines and selfburial. Coast Eng 42(4):213–235

Sutherland AJ (1986) Reports on bridge failure. RRU occasional paper, National Roads Board, Wellington

Tafarojnoruz A, Gaudio R, Dey S (2010) Flow-altering countermeasures against scour at bridge piers: a review. J Hydraul Res 48(4):441–452

Vanoni VA (1975) Sedimentation engineering. ASCE manual number 54, American Society of Civil Engineers, New York

Webby MG (1984) General scour at contraction. RRU bulletin 73, National Roads Board, Bridge Design and Research Seminar, New Zealand, pp 109–118

Yalin MS (1977) Mechanics of sediment transport. Pergamon, Oxford